

EXPLORING HYDROLOGIC RESPONSES TO DIFFERENT
WILDFIRE SPATIAL PATTERNS THROUGH THE LENS OF
COMPUTATIONAL MODELING

by

Luke M. Telfer



A thesis

submitted in partial fulfillment
of the requirements for the degree of
Master of Science in Hydrologic Science
Boise State University

December 2021

© 2021

Luke M. Telfer

ALL RIGHTS RESERVED

BOISE STATE UNIVERSITY GRADUATE COLLEGE

DEFENSE COMMITTEE AND FINAL READING APPROVALS

of the thesis submitted by

Luke M. Telfer

Thesis Title: Exploring hydrologic responses to different wildfire spatial patterns
through the lens of computational modeling

Date of Final Oral Examination: 20 October 2021

The following individuals read and discussed the thesis submitted by student Luke M. Telfer, and they evaluated the student's presentation and response to questions during the final oral examination. They found that the student passed the final oral examination.

Alejandro Flores Ph.D

Chair, Supervisory Committee

Jen Pierce Ph.D

Member, Supervisory Committee

Megan Cattau Ph.D

Member, Supervisory Committee

The final reading approval of the thesis was granted by Alejandro Flores Ph.D, Chair of the Supervisory Committee. The thesis was approved by the Graduate College.

DEDICATION

To Kim and Maddie, for keeping my spirits up during this horrible pandemic.

ACKNOWLEDGMENTS

I would like to thank my advisor, Dr. Lejo Flores, and committee members, Dr. Jen Pierce and Dr. Megan Cattau, for their support and enthusiasm throughout this research; the Boise State University Research Computing team for their assistance and patience with my use of the R2 system; and Ahmad Rezaii for his immense help and guidance while I learned to use the ParFlow-CLM model.

ABSTRACT

Severe wildfire disturbances are becoming increasingly common in high-elevation forests of the western United States. These fires alter watershed hydrologic processes, threatening critical downstream water resources and aquatic ecosystems. However, watershed-scale postfire hydrologic responses and water balance changes are highly uncertain. While postfire effects on individual processes such as runoff, infiltration, evapotranspiration, and snow dynamics are relatively well known, the role of wildfire spatial patterns in governing hydrologic connectivity and interactions between water balance components is poorly understood due to challenges associated with measuring and comparing fires at large scales. This thesis aims to examine pattern-related postfire interactions between various hydrologic processes using computational modeling. Our goals are to identify the primary underlying relationships and to provide a methodological approach upon which a more comprehensive understanding of postfire watershed hydrology can be built.

In Chapter 1, we briefly summarize the current knowledge base regarding postfire hydrology and introduce how hydrologic computational modeling has been used for postfire applications. Chapter 2, written as a manuscript, details the suite of modeling experiments used to explore the effects of wildfire spatial patterns on an idealized, snow-dominated mountain watershed. We used Neutral Landscape Model (NLM) algorithms to generate 150 fire mosaics with varying levels of aggregation and used a

physically-based, distributed model to simulate each mosaic for a full water year. We found that each mosaic created a unique network of flow paths between the burned areas and the watershed outlet and that the size of the network controlled the timing of watershed discharge and soil water storage due to an infiltration capacity gradient between burned and unburned sites. Each fire mosaic generated the same amount of runoff from within the burned areas, but longer flow path networks resulted in more infiltration outside of the fire boundaries. However, because there was enough snow in the watershed to fully saturate the soil in every location, there was little difference in total annual discharge. While these results may be specific to snowmelt-dominated systems, they highlight the importance of considering the entire disturbance flow path network when evaluating watershed-scale postfire hydrologic responses.

TABLE OF CONTENTS

| | |
|--|-----|
| DEDICATION | iv |
| ACKNOWLEDGMENTS | v |
| ABSTRACT | vi |
| LIST OF TABLES | x |
| LIST OF FIGURES | xi |
| LIST OF ABBREVIATIONS | xvi |
| 1 BACKGROUND | 1 |
| 1.1 Introduction | 1 |
| 1.2 Postfire Hydrology | 2 |
| 1.2.1 Fire Terminology and Metrics | 2 |
| 1.2.2 Hydrological Processes | 3 |
| 1.2.3 Spatial Patterns | 7 |
| 1.3 Computational Modeling | 10 |
| 1.3.1 Hydrologic Modeling | 10 |
| 1.3.2 Representing Fire | 12 |
| 1.4 Summary | 13 |

| | |
|---|----|
| References | 15 |
| 2 MODELING POSTFIRE SPATIAL PATTERNS | 25 |
| 2.1 Abstract | 25 |
| 2.2 Introduction | 26 |
| 2.3 Methods | 29 |
| 2.3.1 Model Description | 29 |
| 2.3.2 Study Domain and Model Setup | 30 |
| 2.3.3 Fire Parameterization | 33 |
| 2.3.4 Generating Postfire Landscapes | 35 |
| 2.4 Results | 38 |
| 2.4.1 Controls and Null Predictions | 38 |
| 2.4.2 Variation in Experimental Simulations | 41 |
| 2.4.3 Aggregation and Connectivity | 45 |
| 2.5 Discussion | 47 |
| 2.5.1 Disturbance Flow Path Networks | 47 |
| 2.5.2 Snow-dominated Mountain Watersheds | 50 |
| 2.5.3 Recommended Future Work | 53 |
| 2.6 Conclusion | 54 |
| References | 57 |
| APPENDICES | 70 |
| A METEOROLOGICAL FORCINGS | 70 |
| B POSTFIRE LANDSCAPES | 72 |

| | |
|-------------------------------|----|
| C GITHUB REPOSITORY | 77 |
|-------------------------------|----|

LIST OF TABLES

| | | |
|-----|--|----|
| 1.1 | Example of a fire severity classification scheme modified from Ryan (2002) and Turner <i>et al.</i> (1994) and presented by Keeley (2009). . . . | 3 |
| 2.1 | Parameter values used to distinguish burned and unburned grid cells in ParFlow-CLM. | 34 |
| 2.2 | Mean (SD) contagion values for each experiment group. | 38 |
| C.1 | GitHub repository road map. | 79 |

LIST OF FIGURES

| | | |
|-----|--|----|
| 1.1 | Schematic of the runoff generation mechanism in postfire soils, showing Hortonian overland flow (HOF), saturation overland flow (SOF), and subsurface storm flow (SSSF); from Onda <i>et al.</i> (2008). | 5 |
| 1.2 | Graphical abstract from Ma <i>et al.</i> (2020) showing ET recovery during the first 15 years following fire in the Sierra Nevada of California. . . | 6 |
| 1.3 | Difference between unburned (a,c) and burned (b,d) forested sites from Gleason <i>et al.</i> (2013). (a) and (b) illustrate differences between snow-pack on the same date (May 4, 2012); (c) and (d) show the forest structure as measured by TLS surveys, colored by relative elevation with red being the lowest elevation and green the highest. | 8 |
| 1.4 | Conceptual schematic of ParFlow-CLM for an idealized watershed from Maxwell & Condon (2016). | 11 |
| 1.5 | Compendium of neutral landscape models (Neutral Landscape Models (NLMs)) from Etherington <i>et al.</i> (2015), illustrating the wide variety of process-independent landscape patterns that can be created using computer algorithms. | 13 |
| 2.1 | Location, (a) geology, (b) land cover, and (c) 20-year fire history of the Upper South Fork Salmon River watershed in central Idaho, U.S. . . | 32 |

| | | |
|-----|--|----|
| 2.2 | Examples of the postfire landscapes generated by (a) random, (b) random cluster nearest-neighbor, and (c) midpoint displacement algorithms. | 36 |
| 2.3 | Comparison of watershed-averaged cumulative (a) discharge, (b) change in soil water storage relative to initial conditions, (c) snow water equivalent (SWE), and (d) evapotranspiration (ET) between the two control endmembers: burned (red) and unburned (blue), the null prediction (dotted line), and range of experimental results (green). | 40 |
| 2.4 | Biweekly total (a) discharge, (b) change in soil water storage, (c) snow water equivalent (SWE), and (d) evapotranspiration (ET) for each simulation. Color indicates group membership with green being the least aggregated, blue the most aggregated and orange intermediate. | 42 |
| 2.5 | Timeseries of year-to-date standard deviations between all experiments for discharge, soil water storage, evapotranspiration (ET), and snow water equivalent (SWE). Discharge (blue) is flipped about the y-axis to highlight its relationship with soil water storage and markers indicate snowmelt events and benchmarks that correlate with changes in variability. | 43 |
| 2.6 | Accumulated discharge, change in soil water storage, snow water equivalent (SWE), and evapotranspiration (ET) of each experiment at (a) peak SWE in unburned areas, (b) the snow disappearance date in all areas, and (c) the end of the water year. Color indicates group membership with green being the least aggregated, blue the most aggregated and orange intermediate. | 44 |

| | | |
|-----|---|----|
| 2.7 | (a) Correlation between year-to-date discharge and soil water storage relative to their null predictions at the time of maximum variation. Color indicates the total number of unburned grid cells in the disturbance flow network. Simulations with fewer unburned grid cells in the disturbance flow network have greater discharge and lower soil water storage. (b - e) Disturbance flow network maps corresponding to specific experiments, illustrating the differences in unburned grid cells. | 46 |
| 2.8 | Comparison of disturbance flow path networks between two postfire landscapes generated with the random cluster nearest-neighbor algorithm with similar contagion values. While both have the same number of burned grid cells, (a) has significantly fewer hydrologically connected unburned grid cells than (b). | 49 |
| A.1 | Time series' of mean daily values for each of the eight meteorological forcings used by ParFlow-CLM. | 71 |
| B.1 | Bivariate kernel density estimation plot relating the distribution of contagion values for each experimental group (R, NN, MPD) to the distribution of unburned grid cells contained in their disturbance flow path networks. | 73 |
| B.2 | Map of the disturbance flow path network for each fire mosaic in Group R in ascending order according to the number of unburned grid cells in the network. The brackets above each map show the number of unburned grid cells (left) and the contagion value (right). | 74 |

| | | |
|-----|---|----|
| B.3 | Map of the disturbance flow path network for each fire mosaic in Group NN in ascending order according to the number of unburned grid cells in the network. The brackets above each map show the number of unburned grid cells (left) and the contagion value (right). | 75 |
| B.4 | Map of the disturbance flow path network for each fire mosaic in Group MPD in ascending order according to the number of unburned grid cells in the network. The brackets above each map show the number of unburned grid cells (left) and the contagion value (right). | 76 |

LIST OF ABBREVIATIONS

CLM Community Land Model

dNBR differenced normalized burn ratio

ET evapotranspiration

IGBP International Geosphere-Biosphere Programme

K_{st} saturated hydraulic conductivity

LAI leaf area index

LEAF Lab for Ecohydrology and Applied Forecasting

MTBS Monitoring Trends in Burn Severity

NLM Neutral Landscape Model

SAI stem area index

SSURGO soil survey geographic database

SWE snow water equivalent

USFSR Upper South Fork Salmon River watershed

WRF Weather Research and Forecasting Model

CHAPTER 1: BACKGROUND

1.1 Introduction

Wildfires are ecological disturbances that have helped maintain healthy ecosystems for millions of years by encouraging biodiversity, limiting infestations, and redistributing ecologically important resources (Pausas & Keeley, 2019). However, consequences of climate change such as higher temperatures, prolonged droughts, diminished seasonal snowpack, and earlier spring snowmelt are increasing the frequency and size of high-severity wildfires in many high-elevation forests of the western United States (Dennison *et al.*, 2014; Schoennagel *et al.*, 2004; Westerling, 2006, 2016). This trend represents a threat to critical water supplies and heightens the risk of second-order postfire disturbances such as flooding and mass wasting events (Robinne *et al.*, 2020).

Wildfire modifies important hydrological processes which influence infiltration, evapotranspiration, and runoff; hydrologic responses that impact downstream water resources and endanger human life and property (Hallema *et al.*, 2017). Postfire changes to water quality, quantity, timing, and availability directly affect the more than two-thirds of American municipalities that receive a majority of their drinking water from forests (Bladon *et al.*, 2014). Precipitation events in burned watersheds produce higher flood levels and reduced flood warning times (Neary *et al.*, 2003). Sed-

iment bulking of storm runoff leads to the generation of postfire debris flows, causing 25-50 deaths and over \$2 billion in damage annually (Cannon *et al.*, 2003; Santi *et al.*, 2011). These kinds of societal impacts are expected to worsen as the wildland-urban interface becomes progressively more populated (Radeloff *et al.*, 2005). Managing these risks requires an understanding of how fires influence hydrologic processes at small scales and the manner in which they combine to produce hydrologic responses at larger scales.

1.2 Postfire Hydrology

Wildfire disrupts watershed hydrological processes by consuming vegetation and altering structural and chemical properties of the soil. The combination of a fire's intensity (time-averaged energy flux in units of W m^{-2}) and residence time (duration) determines the degree of impact, which varies in space depending on topography, weather, and the type, amount, and condition of combustible fuels (Certini, 2005; Keeley, 2009). This results in heterogeneous postfire landscapes characterized by complex spatial patterns between different levels of burn severity. The overall hydrologic impact of a fire thus depends on the degree of burn severity in aggregate and may be amplified or moderated by the nature of the fire's spatial patterns.

1.2.1 Fire Terminology and Metrics

Burn severity is a map-able, site-specific measure of disturbance magnitude (Eidenshink *et al.*, 2007). Measurement techniques vary, but typically rely on some combination of remote sensing and field observation. The term is inconsistently applied throughout the literature and, depending on the focus of a particular study, could refer to a fire's effect on vegetation biomass (vegetation burn severity), soil and

surface properties (soil burn severity), or both. Here, we use the unmodified *burn severity* to mean the combined effects pertaining to vegetation and soil.

Table 1.1: Example of a fire severity classification scheme modified from Ryan (2002) and Turner *et al.* (1994) and presented by Keeley (2009).

| Fire severity | Description |
|--|---|
| <i>Unburned</i> | Plant parts green and unaltered, no direct effect from heat |
| <i>Scorched</i> | Unburned but plants exhibit leaf loss from radiated heat |
| <i>Light</i> | Canopy trees with green needles although stems scorched Surface litter, mosses, and herbs charred or consumed Soil organic layer largely intact and charring limited to a few mm depth |
| <i>Moderate of severe surface burn</i> | Trees with some canopy cover killed, but needles not consumed All understory plants charred or consumed Fine dead twigs on soil surface consumed and logs charred Pre-fire soil organic layer largely consumed |
| <i>Deep burning or crown fire</i> | Canopy trees killed and needles consumed Surface litter of all sizes and soil organic layer largely consumed White ash deposition and charred organic matter to several cm depth |

Fire severity, on the other hand, classifies the ecological impact of the fire as a whole. For example, low severity fire is typically characterized by incomplete combustion restricted to the understory and minimal soil damage. High severity fire might consume most or all vegetation on the ground and in the forest canopy and produce significant downward pulses of heat that can penetrate deep into the soil (Keeley, 2009).

1.2.2 Hydrological Processes

Runoff Generation

Wildfire removes and replaces litter and understory vegetation with ash and char (Hallema *et al.*, 2017). Raindrop impacts on the newly exposed soil can cause surface

sealing (Moody *et al.*, 2013), either by encrusting the surface through ash compaction or by dislocating and forcing smaller particles into soil pores (Gabet & Sternberg, 2008). Surface-sealing effects may also occur if the deposited ash has lower hydraulic conductivity than the underlying soil (Woods & Balfour, 2010).

Additionally, near-surface combustion sends pulses of heat into the soil that can cause (or enhance) hydrophobicity in the uppermost soil layers (Doerr *et al.*, 2006). Fire-induced hydrophobicity is thought to be caused by pyrolysis and volatilization of organic compounds present in the soil (Hallema *et al.*, 2017). These compounds move downward along the thermal gradient before condensing as a water repellent layer parallel to the soil surface (DeBano, 2000).

Surface sealing and water repellent layers reduce infiltration rates by restricting sorptivity, wetting front potential, and soil hydraulic conductivity (Ebel *et al.*, 2012). This increases the likelihood of surface ponding during subsequent precipitation, even for relatively low intensity events (Maina & Siirila-Woodburn, 2019). The absence of litter and understory vegetation also reduces the ability to store surface water and removes obstructions to flow which, combined with the lower infiltration capacity, generally increases surface runoff following a fire (Larsen *et al.*, 2009).

Furthermore, moderate and high severity fires are capable of consuming overstory vegetation. This results in greater net precipitation by decreasing interception and canopy evaporation (Williams *et al.*, 2014). Unburned trees and shrubs can intercept as much as 50% of rainfall by volume (Stoof *et al.*, 2012) and their loss may effectively double net precipitation. The resulting increase in water availability at the surface is another factor responsible for increased runoff generation.

While the loss of canopy cover can take decades to recover, reduced infiltration

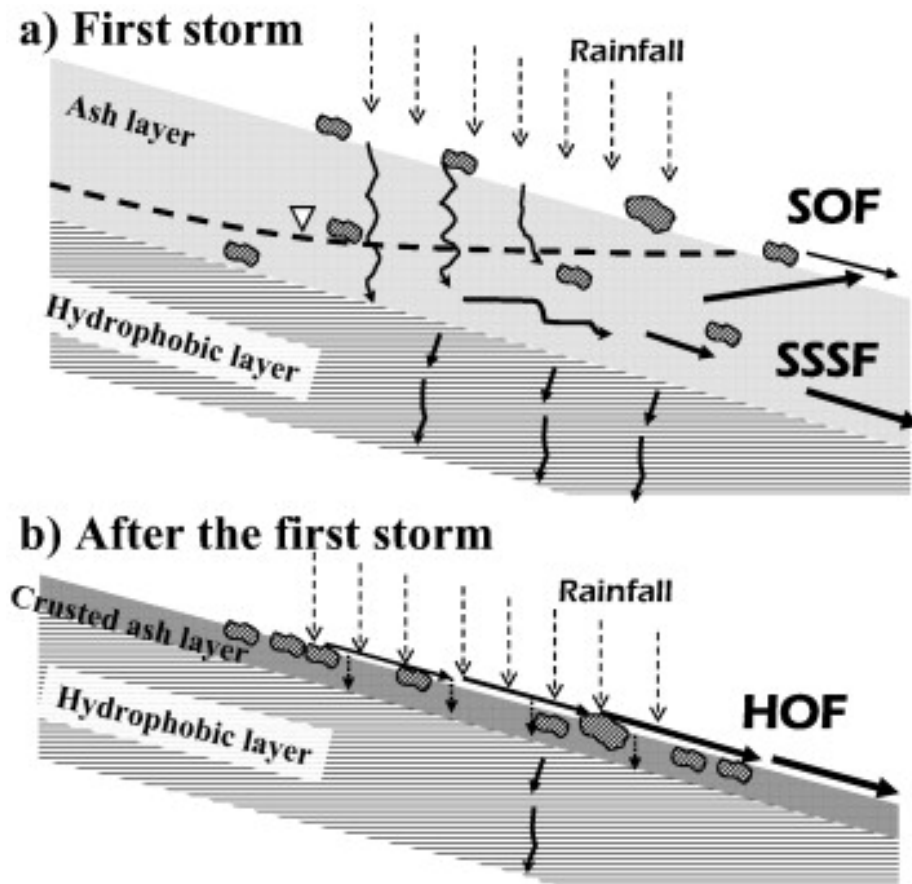


Figure 1.1: Schematic of the runoff generation mechanism in postfire soils, showing Hortonian overland flow (HOF), saturation overland flow (SOF), and subsurface storm flow (SSSF); from Onda *et al.* (2008).

does not typically persist beyond a couple of years postfire. Soil water repellency approaches prefire levels after one or two years (MacDonald & Huffman, 2004), whereas ash cover may be washed out or removed by wind erosion within the first month postfire (Bodí *et al.*, 2014). Thus, increases in runoff generation attributable to changes in infiltration are most significant during the first few postfire storms.

Evapotranspiration

Vegetation mortality lowers biological water demand, reducing both total evapotranspiration (ET) (Dore *et al.*, 2012) and the evapotranspiration-to-precipitation ratio (Poon & Kinoshita, 2018). This may lead to increased soil moisture in severely burned sites despite the short-term reduction in infiltration capacity (Cardenas & Kanarek, 2014). Sites with higher vegetation burn severity and/or greater prefire vegetation density experience larger reductions in ET (Ma *et al.*, 2020).

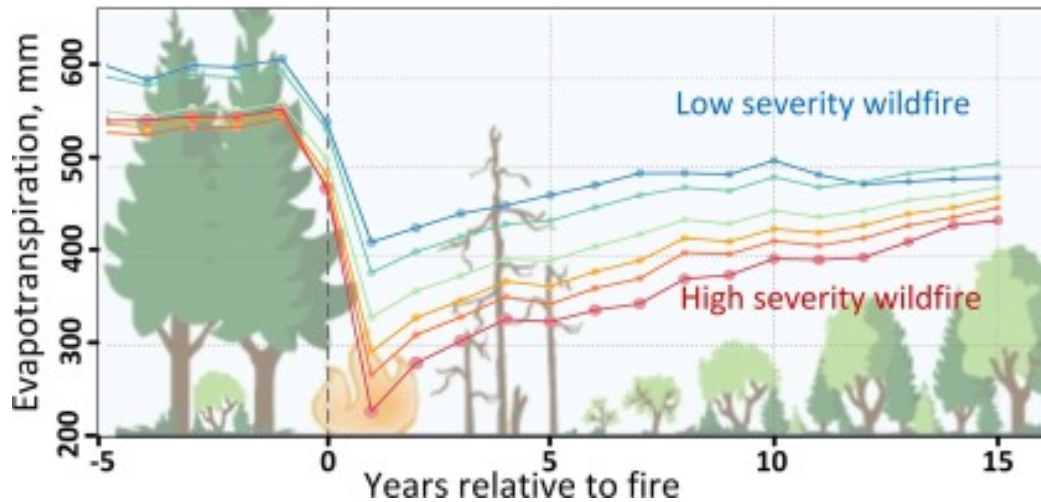


Figure 1.2: Graphical abstract from Ma *et al.* (2020) showing ET recovery during the first 15 years following fire in the Sierra Nevada of California.

Vegetation recovery has an ameliorative effect on ET but occurs slowly over several years, especially in high burn severity sites (Kinoshita & Hogue, 2011). Ma *et al.* (2020) – in examining the effects of wildfire on ET across California’s Sierra Nevada – found that low severity and high severity sites reduced ET by 31% and 50%, respectively, in the first year following the fire. After 15 years, few sites had completely recovered and the total ET over that time frame was 23% lower (Fig. 1.2).

Snow Dynamics

The loss of canopy vegetation also disrupts snow processes in mountainous watersheds. Snow accumulation in response to wildfire varies considerably across studies, from a 10% decrease to a 50% increase (Maxwell *et al.*, 2019). Studies showing increased peak SWE in burned areas point to reduced interception and thereby less canopy sublimation as the primary cause (Burles & Boon, 2011; Gleason *et al.*, 2013). Alternatively, greater wintertime ablation and wind redistribution may be the more dominant processes where peak SWE was shown to decrease following fire (Harpold *et al.*, 2014). Maxwell *et al.* (2019) suggests that other variables, such as weather, topography, and potentially latitude, are needed to explain postfire snow accumulation response.

Snow melt, on the other hand, consistently occurs earlier and at a greater rate in burned areas throughout the literature. Canopy removal results in more incident sunlight reaching the snow surface (Burles & Boon, 2011), greater exposure to turbulent fluxes (Maxwell *et al.*, 2019) and the deposition of fire byproducts like black carbon reduces snow albedo (Gleason *et al.*, 2013). Gleason *et al.* (2019) investigated postfire radiative forcing on snow across the American West and conservatively estimated that these factors increase the daily solar energy absorption by around 400%. This causes earlier onset of snow melt and faster ablation rates, culminating in snow disappearance 19 ± 9 days earlier on average (Uecker *et al.*, 2020).

1.2.3 Spatial Patterns

Hydrologic connectivity describes how spatial relationships between distributed landscape elements influence water transfer pathways and flow patterns, including

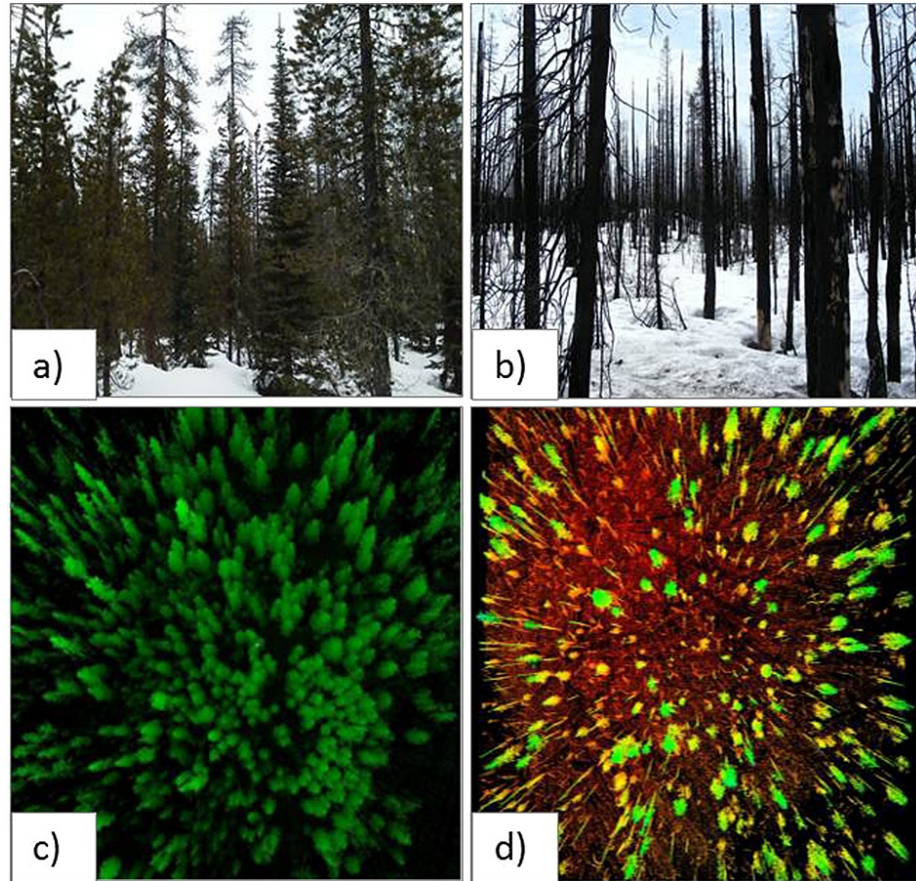


Figure 1.3: Difference between unburned (a,c) and burned (b,d) forested sites from Gleason *et al.* (2013). (a) and (b) illustrate differences between snowpack on the same date (May 4, 2012); (c) and (d) show the forest structure as measured by TLS surveys, colored by relative elevation with red being the lowest elevation and green the highest.

related sediment movement (Lexartza-Artza & Wainwright, 2009). Wildfire generally increases the preexisting hydrologic connectivity by creating new pathways and removing landscape elements that inhibit flow. Moreover, because postfire landscapes are heterogeneous mosaics of different fire severities, the spatial arrangement of varying fire effects can amplify or dampen the overall hydrologic and geomorphic impacts (Cawson *et al.*, 2013; Hooke *et al.*, 2017; Kutiel *et al.*, 1995; Lavee *et al.*, 1995; Moody *et al.*, 2008).

Such spatial relationships are complex and research regarding postwildfire hydrologic connectivity is relatively sparse, especially at the watershed scale (Hallema *et al.*, 2017). Most studies have examined the relationship between wildfire and hydrologic connectivity through the lens of erosion and sediment pathways at the hillslope scale (Cawson *et al.*, 2013; Kutiel *et al.*, 1995; Lavee *et al.*, 1995; Wester *et al.*, 2014; Williams *et al.*, 2015; Wilson *et al.*, 2021) and some in the context of ecological restoration at the watershed scale (López-Vicente & Martínez-Murillo, 2016; Maia *et al.*, 2012). Few have looked specifically at the effects on hydrological processes themselves (Moody *et al.*, 2008; Ortíz-Rodríguez *et al.*, 2019).

In simulated rainfall-runoff experiments, Lavee *et al.* (1995) found that patchy, heterogeneous postfire hillslopes were composed of runoff contributing and runoff accepting zones which caused discontinuous overland flow and sediment movement. Overland flow generated in one area was quickly infiltrated upon reaching a higher permeability, unburned or low severity patch. Similarly, in a study directly manipulating prescribed burns, Cawson *et al.* (2013) observed that unburned patches were particularly effective at limiting postfire runoff and erosion for eucalypt forests in Australia. Also using prescribed burns, Williams *et al.* (2015) demonstrated that the magnitude of hydrologic response is controlled by the degree of cross-scale structural and functional connectivity in terms of surface susceptibility, runoff and erosion processes, and sediment availability.

Moody *et al.* (2008) developed a burn severity variable, *hydraulic functional connectivity*, that relates differenced normalized burn ratio (dNBR) to hillslope runoff processes and found that the magnitude and spatial sequences of soil burn severities along hillslope flowpaths was linearly related to runoff in the 2000 Cerro Grande

Fire near Los Alamos, New Mexico. Higher burn severities near the main channel generated more runoff than higher burn severities near the catchment divide, despite the flow paths having similar aggregate severities. Watershed hydraulic functional connectivity thus provides a first order description of how burn severity patterns are imprinted over the drainage network.

1.3 Computational Modeling

Wildfire's impact on watershed-scale hydrological systems – especially with regard to the consequences of spatial patterns – is difficult to study due to the scarcity of site specific data from before and after a fire; high costs associated with large-scale, field-based studies; and temporal and location comparability issues between fires due to differences in terrain, weather, prefire vegetation, etc. In recent years, increasingly complex computational models have been used to overcome these limitations and gain further insight into watershed postfire hydrology.

1.3.1 Hydrologic Modeling

A common approach is change detection modeling, which models watershed hydrology as if a fire never occurred and compares the output to actual postfire hydrologic measurements (Seibert & van Meerveld, 2016). Most change detection studies use lumped models (where spatial variations are averaged or ignored) and seek to coarsely quantify the hydrologic change caused by a specific wildfire disturbance. This approach is inherently incapable of identifying the role of burn severity spatial configuration.

Distributed models, on the other hand, explicitly consider spatial variations of characteristics and processes (Feldman, 2000). This makes them appropriate for

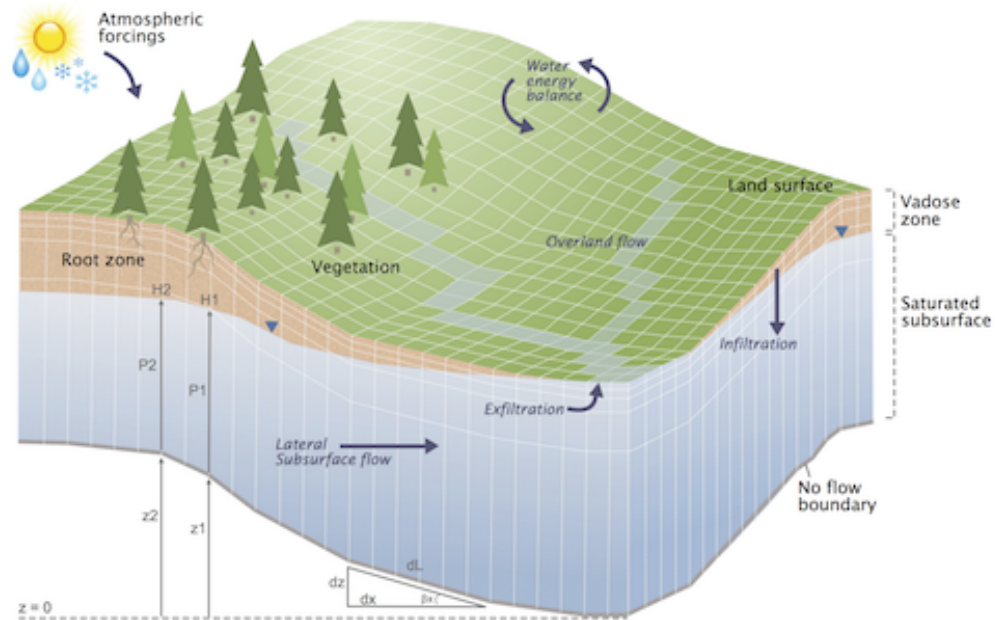


Figure 1.4: Conceptual schematic of ParFlow-CLM for an idealized watershed from Maxwell & Condon (2016).

investigating the impact of burn severity heterogeneity. The ParFlow-Community Land Model (CLM) in particular has been used in a number of recent watershed scale disturbance studies (Penn *et al.*, 2016; Lopez *et al.*, 2016; Escobar *et al.*, 2017; Maina & Siirila-Woodburn, 2019). ParFlow simulates critical zone water and energy transfers and is coupled to CLM, which accounts for the spatial distribution of land surface and vegetation processes (Maina & Siirila-Woodburn, 2019). By modeling the postfire landscape rather than a hypothetically unburned landscape (as with change detection modeling), these kinds of studies are able to achieve greater resolution and observe dynamic processes and interactions between water budget components.

1.3.2 Representing Fire

Investigating postfire hydrologic systems with process-based modeling requires the representation of burned regions and the hydrologically relevant fire effects within those regions. Burned areas are either hypothetical or defined by the boundary of some historical fire of interest. Updated model parameters designed to emulate fire effects are then mapped to the burned area with parameterization schemes ranging from simple “barren soil” representations to spatially distributed ones that relate dNBR to soil and vegetation changes.

Nearly all studies modeling postfire hydrology used historical fires to define and parameterize burned areas. For example, Atchley *et al.* (2018) used ParFlow-CLM to evaluate postfire water balance progression for the 2011 Las Conchas fire in New Mexico. Here, the leaf area index (LAI) parameter – which determines both the canopy extent and amount of biomass – was manipulated in order to represent a range of vegetation burn severities. Soil burn severity was also represented by relating the saturated hydraulic conductivity (K_{st}) value in the top two centimeters of the soil to dNBR in accordance with the relationship developed by Moody *et al.* (2015). Although fire influences multiple infiltration parameters, K_{st} was assumed to capture their combined effect and was noted by Ebel *et al.* (2016) as the dominant soil hydrologic property change postfire.

Few postfire hydrology studies have used hypothetical burned areas. Many, like Maina & Siirila-Woodburn (2019), elected to use historical boundaries in order to preserve realism and reduce uncertainty. Ecological studies, however, commonly use artificial landscapes produced by analytical algorithms to study ecological responses to landscape patterns. These models — known as neutral landscape models (NLMs)

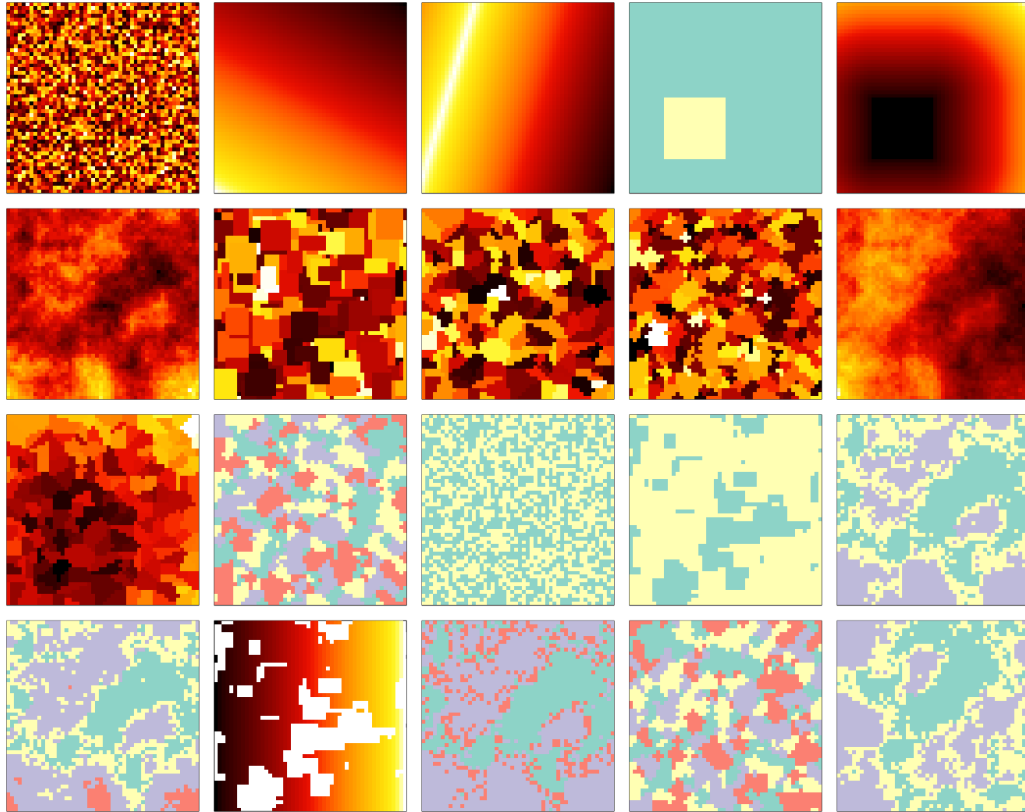


Figure 1.5: Compendium of neutral landscape models (NLMs) from Etherington *et al.* (2015), illustrating the wide variety of process-independent landscape patterns that can be created using computer algorithms.

because they are independent from the biological and physical processes that shape actual landscape patterns (McGarigal, 2015) — are used to conduct highly controlled experiments at scales where real-world experiments are logistically impractical. NLMs have been used to represent wildfire disturbances in an ecological context (Keane *et al.*, 2013) and appear well-suited for postfire hydrological studies.

1.4 Summary

A notable opportunity for advancing postfire hydrology lies with studying the impact of wildfire spatial heterogeneity. The relationship between burn severity and

postfire critical zone properties is well-documented through field and laboratory experiments (Certini, 2005), and change detection modeling has broadly characterized postfire watershed behavior after the fact (Seibert & van Meerveld, 2016). Hillslope-scale studies indicate that spatial patterns of burn severity play a significant role in determining both hydrologic and geomorphic responses (Moody *et al.*, 2008; Cawson *et al.*, 2013), but the contribution of these patterns at the watershed scale is poorly understood for a variety of reasons. Field-based empirical studies at this scale are prohibitively difficult (Hallema *et al.*, 2017) and physically-based hydrologic models generally lack the ability to account for wildfires. Those that do typically treat fire as a homogeneously burned area (Maina & Siirila-Woodburn, 2019) and seek to predict the occurrence or rate of spread rather than postfire heterogeneity (Zou *et al.*, 2019).

The watershed scale is where postfire flooding, erosion, and sedimentation issues occur and where mitigation practices are implemented. For these reasons, Hallema *et al.* (2017) identifies the need for more watershed scale assessments as a grand challenge in hydrology. Watershed scale assessments require upscaling of field data (necessitating large numbers of pre- and post-wildfire experiments) and obtaining the required measurements is a logistical challenge because predicting the locations of future wildfires is difficult, let alone suitable measurement sites.

References

- Atchley, Adam L., Kinoshita, Alicia M., Lopez, Sonya R., Trader, Laura, & Middleton, Richard. 2018. Simulating Surface and Subsurface Water Balance Changes Due to Burn Severity. *Vadose Zone Journal*, **17**(1), 0.
- Bladon, Kevin D., Emelko, Monica B., Silins, Uldis, & Stone, Micheal. 2014. Wildfire and the Future of Water Supply. *Environmental Science & Technology*, **48**(16), 8936–8943.
- Bodí, Merche B, Martin, Deborah A, Balfour, Victoria N, Santín, Cristina, Doerr, Stefan H, Pereira, Paulo, Cerdà, Artemi, & Mataix-Solera, Jorge. 2014. Wildland fire ash: production, composition and eco-hydro-geomorphic effects. *Earth-Science Reviews*, **130**, 103–127.
- Burles, Katie, & Boon, Sarah. 2011. Snowmelt energy balance in a burned forest plot, Crowsnest Pass, Alberta, Canada. *Hydrological processes*, **25**(19), 3012–3029.
- Cannon, S H, Gartner, J E, Parrett, C, & Parise, M. 2003. Wildfire-related debris-flow generation through episodic progressive sediment-bulking processes, western USA. 12.
- Cardenas, M Bayani, & Kanarek, Michael R. 2014. Soil moisture variation and dynamics across a wildfire burn boundary in a loblolly pine (*Pinus taeda*) forest. *Journal of hydrology*, **519**, 490–502.
- Cawson, J.G., Sheridan, G.J., Smith, H.G., & Lane, P.N.J. 2013. Effects of fire

- severity and burn patchiness on hillslope-scale surface runoff, erosion and hydrologic connectivity in a prescribed burn. *Forest Ecology and Management*, **310**(Dec.), 219–233.
- Certini, Giacomo. 2005. Effects of fire on properties of forest soils: a review. *Oecologia*, **143**(1), 1–10.
- DeBano, Leonard F. 2000. The role of fire and soil heating on water repellency in wildland environments: a review. *Journal of hydrology*, **231**, 195–206.
- Dennison, Philip E., Brewer, Simon C., Arnold, James D., & Moritz, Max A. 2014. Large wildfire trends in the western United States, 1984-2011: DENNISON ET. AL.; LARGE WILDFIRE TRENDS IN THE WESTERN US. *Geophysical Research Letters*, **41**(8), 2928–2933.
- Doerr, S.H., Shakesby, R.A., Blake, W.H., Chafer, C.J., Humphreys, G.S., & Wallbrink, P.J. 2006. Effects of differing wildfire severities on soil wettability and implications for hydrological response. *Journal of Hydrology*, **319**(1-4), 295–311.
- Dore, Sabina, Montes-Helu, Mario, Hart, Stephen C., Hungate, Bruce A., Koch, George W., Moon, John B., Finkral, Alex J., & Kolb, Thomas E. 2012. Recovery of ponderosa pine ecosystem carbon and water fluxes from thinning and stand-replacing fire. *Global Change Biology*, **18**(10), 3171–3185.
- Ebel, Brian A, Moody, John A, & Martin, Deborah A. 2012. Hydrologic conditions controlling runoff generation immediately after wildfire. *Water Resources Research*, **48**(3).

- Ebel, Brian A, Rengers, Francis K, & Tucker, Gregory E. 2016. Observed and simulated hydrologic response for a first-order catchment during extreme rainfall 3 years after wildfire disturbance. *Water Resources Research*, **52**(12), 9367–9389.
- Eidenshink, Jeff, Schwind, Brian, Brewer, Ken, Zhu, Zhi-Liang, Quayle, Brad, & Howard, Stephen. 2007. A Project for Monitoring Trends in Burn Severity. *Fire Ecology*, **3**(1), 3–21.
- Escobar, Isabel S, Lopez, Sonya R, & Kinoshita, Alicia M. 2017. Modeling post-wildfire hydrological processes with ParFlow. *In: AGU Fall Meeting Abstracts*.
- Etherington, Thomas R, Holland, E Penelope, & O’Sullivan, David. 2015. NLM py: a python software package for the creation of neutral landscape models within a general numerical framework. *Methods in Ecology and Evolution*, **6**(2), 164–168.
- Feldman, Arlen D. 2000. *Hydrologic modeling system HEC-HMS: technical reference manual*. US Army Corps of Engineers, Hydrologic Engineering Center.
- Gabet, Emmanuel J, & Sternberg, Paul. 2008. The effects of vegetative ash on infiltration capacity, sediment transport, and the generation of progressively bulked debris flows. *Geomorphology*, **101**(4), 666–673.
- Gleason, Kelly E, Nolin, Anne W, & Roth, Travis R. 2013. Charred forests increase snowmelt: Effects of burned woody debris and incoming solar radiation on snow ablation. *Geophysical Research Letters*, **40**(17), 4654–4661.
- Gleason, Kelly E., McConnell, Joseph R., Arienzo, Monica M., Chellman, Nathan, & Calvin, Wendy M. 2019. Four-fold increase in solar forcing on snow in western U.S. burned forests since 1999. *Nature Communications*, **10**(1), 2026.

- Hallema, Dennis W., Sun, Ge, Bladon, Kevin D., Norman, Steven P., Caldwell, Peter V., Liu, Yongqiang, & McNulty, Steven G. 2017. Regional patterns of post-wildfire streamflow response in the Western United States: The importance of scale-specific connectivity. *Hydrological Processes*, **31**(14), 2582–2598.
- Harpold, Adrian A, Biederman, Joel A, Condon, Katherine, Merino, Manuel, Korgaonkar, Yoganand, Nan, Tongchao, Sloat, Lindsey L, Ross, Morgan, & Brooks, Paul D. 2014. Changes in snow accumulation and ablation following the Las Conchas Forest Fire, New Mexico, USA. *Ecohydrology*, **7**(2), 440–452.
- Hooke, Janet, Sandercock, Peter, Cammeraat, LH, Lesschen, Jan Peter, Borselli, Lorenzo, Torri, Dino, Meerkerk, André, van Wesemael, Bas, Marchamalo, Miguel, Barbera, Gonzalo, *et al.* 2017. Mechanisms of degradation and identification of connectivity and erosion hotspots. *Pages 13–37 of: Combating Desertification and Land Degradation*. Springer.
- Keane, Robert E, Cary, Geoffrey J, Flannigan, Mike D, Parsons, Russell A, Davies, Ian D, King, Karen J, Li, Chao, Bradstock, Ross A, & Gill, Malcolm. 2013. Exploring the role of fire, succession, climate, and weather on landscape dynamics using comparative modeling. *Ecological Modelling*, **266**, 172–186.
- Keeley, Jon E. 2009. Fire intensity, fire severity and burn severity: a brief review and suggested usage. *International Journal of Wildland Fire*, **18**(1), 116.
- Kinoshita, Alicia M., & Hogue, Terri S. 2011. Spatial and temporal controls on post-fire hydrologic recovery in Southern California watersheds. *CATENA*, **87**(2), 240–252.

- Kutiel, P, Lavee, H, Segev, M, & Benyamini, Y. 1995. The effect of fire-induced surface heterogeneity on rainfall-runoff-erosion relationships in an eastern Mediterranean ecosystem, Israel. *Catena*, **25**(1-4), 77–87.
- Larsen, Isaac J, MacDonald, Lee H, Brown, Ethan, Rough, Daniella, Welsh, Matthew J, Pietraszek, Joseph H, Libohova, Zamir, de Dios Benavides-Solorio, Juan, & Schaffrath, Keelin. 2009. Causes of post-fire runoff and erosion: Water repellency, cover, or soil sealing? *Soil Science Society of America Journal*, **73**(4), 1393–1407.
- Lavee, H, Kutiel, P, Segev, M, & Benyamini, Y. 1995. Effect of surface roughness on runoff and erosion in a Mediterranean ecosystem: the role of fire. *Geomorphology*, **11**(3), 227–234.
- Lexartza-Artza, Irantzu, & Wainwright, John. 2009. Hydrological connectivity: Linking concepts with practical implications. *Catena*, **79**(2), 146–152.
- Lopez, Sonya R, Kinoshita, Alicia M, & Atchley, Adam Lee. 2016. Evaluating post-wildfire hydrologic recovery using ParFlow in southern California. *In: AGU Fall Meeting Abstracts*.
- López-Vicente, Manuel, & Martínez-Murillo, Juan F. 2016. Modelling hydrological connectivity in burned areas. A case study from South of Spain.
- Ma, Qin, Bales, Roger C, Rungee, Joseph, Conklin, Martha H, Collins, Brandon M, & Goulden, Michael L. 2020. Wildfire controls on evapotranspiration in California's Sierra Nevada. *Journal of Hydrology*, **590**, 125364.

- MacDonald, Lee H, & Huffman, Edward L. 2004. Post-fire soil water repellency: persistence and soil moisture thresholds. *Soil Science Society of America Journal*, **68**(5), 1729–1734.
- Maia, Paula, Pausas, Juli G, Vasques, Ana, & Keizer, Jan Jacob. 2012. Fire severity as a key factor in post-fire regeneration of *Pinus pinaster* (Ait.) in Central Portugal. *Annals of forest science*, **69**(4), 489–498.
- Maina, Fadji Zaoua, & Siirila-Woodburn, Erica R. 2019. Watersheds dynamics following wildfires: Nonlinear feedbacks and implications on hydrologic responses. *Hydrological Processes*, Aug., hyp.13568.
- Maxwell, Jordan D, Call, Anson, & Clair, Samuel B St. 2019. Wildfire and topography impacts on snow accumulation and retention in montane forests. *Forest ecology and management*, **432**, 256–263.
- Maxwell, Reed M, & Condon, Laura E. 2016. Connections between groundwater flow and transpiration partitioning. *Science*, **353**(6297), 377–380.
- McGarigal, Kevin. 2015. FRAGSTATS help. *University of Massachusetts: Amherst, MA, USA*, 182.
- Moody, John A., Martin, Deborah A., Haire, Sandra L., & Kinner, David A. 2008. Linking runoff response to burn severity after a wildfire. *Hydrological Processes*, **22**(13), 2063–2074.
- Moody, John A., Shakesby, Richard A., Robichaud, Peter R., Cannon, Susan H., & Martin, Deborah A. 2013. Current research issues related to post-wildfire runoff and erosion processes. *Earth-Science Reviews*, **122**(July), 10–37.

- Moody, John A, Ebel, Brian A, Nyman, Petter, Martin, Deborah A, Stoof, Cathelijne, & McKinley, Randy. 2015. Relations between soil hydraulic properties and burn severity. *International Journal of Wildland Fire*, **25**(3), 279–293.
- Neary, Daniel G, Gottfried, Gerald J, & Ffolliott, Peter F. 2003. POST-WILDFIRE WATERSHED FLOOD RESPONSES. 9.
- Onda, Yuichi, Dietrich, William E, & Booker, Fred. 2008. Evolution of overland flow after a severe forest fire, Point Reyes, California. *Catena*, **72**(1), 13–20.
- Ortíz-Rodríguez, Azalea Judith, Muñoz-Robles, Carlos, & Borselli, Lorenzo. 2019. Changes in connectivity and hydrological efficiency following wildland fires in Sierra Madre Oriental, Mexico. *Science of the Total Environment*, **655**, 112–128.
- Pausas, Juli G, & Keeley, Jon E. 2019. Wildfires as an ecosystem service. *Frontiers in Ecology and the Environment*, **17**(5), 289–295.
- Penn, Colin A, Bearup, Lindsay A, Maxwell, Reed M, & Clow, David W. 2016. Numerical experiments to explain multiscale hydrological responses to mountain pine beetle tree mortality in a headwater watershed. *Water Resources Research*, **52**(4), 3143–3161.
- Poon, Patrick K, & Kinoshita, Alicia M. 2018. Spatial and temporal evapotranspiration trends after wildfire in semi-arid landscapes. *Journal of hydrology*, **559**, 71–83.
- Radeloff, Volker C, Hammer, Roger B, Stewart, Susan I, Fried, Jeremy S, Holcomb, Sherry S, & McKeefry, Jason F. 2005. The wildland–urban interface in the United States. *Ecological applications*, **15**(3), 799–805.

- Robinne, François-Nicolas, Hallema, Dennis W, Bladon, Kevin D, & Buttle, James M. 2020. Wildfire impacts on hydrologic ecosystem services in North American high-latitude forests: A scoping review. *Journal of Hydrology*, **581**, 124360.
- Ryan, Kevin C. 2002. Dynamic interactions between forest structure and fire behavior in boreal ecosystems. *Silva Fennica*, **36**(1), 13–39.
- Santi, P. M., Hewitt, K., VanDine, D. F., & Barillas Cruz, E. 2011. Debris-flow impact, vulnerability, and response. *Natural Hazards*, **56**(1), 371–402.
- Schoennagel, Tania, Veblen, Thomas T., & Romme, William H. 2004. The Interaction of Fire, Fuels, and Climate across Rocky Mountain Forests. *BioScience*, **54**(7), 661.
- Seibert, Jan, & van Meerveld, H.J. Ilja. 2016. Hydrological change modeling: Challenges and opportunities: Invited Commentary. *Hydrological Processes*, **30**(26), 4966–4971.
- Stoof, Cathelijne R, Vervoort, RW, Iwema, J, Elsen, E, Ferreira, AJD, & Ritsema, CJ. 2012. Hydrological response of a small catchment burned by experimental fire. *Hydrology and Earth System Sciences*, **16**(2), 267–285.
- Turner, Monica G, Hargrove, William W, Gardner, Robert H, & Romme, William H. 1994. Effects of fire on landscape heterogeneity in Yellowstone National Park, Wyoming. *Journal of Vegetation Science*, **5**(5), 731–742.
- Uecker, Ted M, Kaspari, Susan D, Musselman, Keith N, & McKenzie Skiles, S. 2020. The Post-Wildfire Impact of Burn Severity and Age on Black Carbon Snow Deposition and Implications for Snow Water Resources, Cascade Range, Washington. *Journal of Hydrometeorology*, **21**(8), 1777–1792.

- Wester, Thad, Wasklewicz, Thad, & Staley, Dennis. 2014. Functional and structural connectivity within a recently burned drainage basin. *Geomorphology*, **206**, 362–373.
- Westerling, A. L. 2006. Warming and Earlier Spring Increase Western U.S. Forest Wildfire Activity. *Science*, **313**(5789), 940–943.
- Westerling, Anthony LeRoy. 2016. Increasing western US forest wildfire activity: sensitivity to changes in the timing of spring. *Philosophical Transactions of the Royal Society B: Biological Sciences*, **371**(1696), 20150178.
- Williams, C. Jason, Pierson, Frederick B., Robichaud, Peter R., & Boll, Jan. 2014. Hydrologic and erosion responses to wildfire along the rangeland–xeric forest continuum in the western US: a review and model of hydrologic vulnerability. *International Journal of Wildland Fire*, **23**(2), 155.
- Williams, C Jason, Pierson, Frederick B, Robichaud, Peter R, Al-Hamdan, Osama Z, Boll, Jan, & Strand, Eva K. 2015. Structural and functional connectivity as a driver of hillslope erosion following disturbance. *International Journal of Wildland Fire*, **25**(3), 306–321.
- Wilson, Codie, Kampf, Stephanie K, Ryan, Sandra, Covino, Tim, MacDonald, Lee H, & Gleason, Hunter. 2021. Connectivity of post-fire runoff and sediment from nested hillslopes and watersheds. *Hydrological Processes*, **35**(1), e13975.
- Woods, Scott W, & Balfour, Victoria N. 2010. The effects of soil texture and ash thickness on the post-fire hydrological response from ash-covered soils. *Journal of Hydrology*, **393**(3-4), 274–286.

Zou, Yufei, Wang, Yuhang, Ke, Ziming, Tian, Hanqin, Yang, Jia, & Liu, Yongqiang. 2019. Development of a REgion-specific ecosystem feedback fire (RESFire) model in the Community Earth System Model. *Journal of Advances in Modeling Earth Systems*, **11**(2), 417–445.

CHAPTER 2:

MODELING POSTFIRE SPATIAL PATTERNS

2.1 Abstract

Wildfires disrupt watershed hydrologic processes by removing vegetation and altering soil properties, threatening downstream water resources and increasing the risk of destructive postfire erosion, debris flows, and flooding. Plot-scale postfire effects on runoff, infiltration, and evapotranspiration are well-documented; yet watershed-scale hydrologic responses remain highly uncertain. Part of this uncertainty lies with a poor understanding of how postfire spatial patterns influence water transfer pathways and flow patterns due to challenges associated with measuring and comparing wildfire disturbances. In this study, we use a physically-based hydrologic model to simulate an idealized, snow-dominated mountain watershed under a controlled suite of postfire landscape patterns. We found that a fire's spatial arrangement determined the size of its disturbance flow path network, defined as the burned area and all hydrologically-connected unburned sites. The size of the disturbance flow path network controlled the timing of watershed discharge and changes in soil water storage. Variation between experiments was driven by earlier snowmelt in burned areas; but the critical pattern-related interactions took place outside the fire boundaries in unburned parts of the disturbance network. Considering these indirectly affected unburned regions in

postfire assessments would likely improve predictions of hydrologic responses at the watershed scale.

2.2 Introduction

Large, high-severity wildfires are becoming more common in the mountain forests of the western United States due to recurrent drought, rising temperatures, and fuel accumulation from fire-exclusion practices (Collins *et al.*, 2017; Dennison *et al.*, 2014; Littell *et al.*, 2016; Westerling, 2006, 2016). Such fires can drastically alter watershed hydrologic processes by removing vegetation and damaging the soil to a degree that increases the risk of postfire debris flows and flooding and threatens downstream water resources and aquatic ecosystems (Bladon *et al.*, 2014; Cannon *et al.*, 2003; Murphy *et al.*, 2019; Sankey *et al.*, 2017; Santi *et al.*, 2011).

These impacts are particularly concerning given the progressively populated wildland-urban interface (Radeloff *et al.*, 2005) and the fact that forests provide 65% of the water supply in the western United States (Furniss, 2010; Hallema *et al.*, 2017). Postfire hydrologic responses are also highly variable and difficult to predict; being dependent on climatic conditions, soil and vegetation burn severity magnitudes, topography, and changes to hydrologic connectivity (Cawson *et al.*, 2013; Hallema *et al.*, 2018; Shakesby & Doerr, 2006). This indicates an urgent need for developing a comprehensive, detailed understanding of how the manner in which fire effects are imprinted over the landscape influences hydrologic processes and water balance partitioning (Kinoshita *et al.*, 2016; Martin, 2016), especially at watershed scales (Hallema *et al.*, 2017) and complementary to recent postfire sedimentation studies (Murphy *et al.*, 2019; Sankey *et al.*, 2017).

Postfire changes to hydrologic properties and processes at plot and hillslope scales

are well-documented through field and laboratory experiments (Certini, 2005) and have demonstrated general trends in increased runoff and erosion (e.g. Benavides-Solorio & MacDonald, 2001; Kinoshita & Hogue, 2015; Moody & Martin, 2001; Onda *et al.*, 2008; Spigel & Robichaud, 2007), reduced evapotranspiration (ET) leading to greater soil moisture (e.g. Cardenas & Kanarek, 2014; Ma *et al.*, 2020; Poon & Kinoshita, 2018), and changes in snow dynamics (e.g. Burles & Boon, 2011; Gleason *et al.*, 2013; Harpold *et al.*, 2014; Maxwell *et al.*, 2019) within burned areas. However, the role of postfire spatial patterns in influencing hydrologic connectivity and water balance partitioning has received considerably less attention. Wildfire's impact on watershed-scale hydrological systems – especially with regard to the effect of spatial patterns – is difficult to study due to the scarcity of site specific data from before and after a fire (Seibert *et al.*, 2010); high costs associated with large-scale, field-based studies; and comparability issues between individual fire disturbances.

Many studies that have examined the relationship between wildfire and hydrologic connectivity have done so through the lens of erosion and sediment pathways at the hillslope scale (e.g. Cawson *et al.*, 2013; Wester *et al.*, 2014; Williams *et al.*, 2016; Wilson *et al.*, 2021) and some in the context of ecological restoration at the watershed scale (e.g. López-Vicente & Martínez-Murillo, 2016; Maia *et al.*, 2012). Fewer have looked at the effects on hydrological processes themselves (e.g. Moody *et al.*, 2008; Ortíz-Rodríguez *et al.*, 2019), specifically focusing on rainfall-runoff relationships. While these studies indicate that postfire spatial patterns play a significant role in determining hydrologic responses by enhancing or obstructing flow pathways, the watershed-scale impact is poorly understood and consequences for other components of the water balance are only implied.

Given the aforementioned limitations associated with watershed-scale postfire observational studies, high-performance computational modeling could be an important tool for advancing our understanding of such topics. Several modeling frameworks have previously been used to explore postfire hydrology but many of them are limited in their ability to physically capture the surface and subsurface hydrologic processes involved. For example, one approach similar to paired catchment studies (Andréassian *et al.*, 2012) is change detection modeling, which compares observed postfire metrics such as streamflow with values obtained by modeling the hypothetically undisturbed watershed (Seibert & van Meerveld, 2016). This type of approach seeks to quantify the degree of hydrologic change but does not address the processes involved in achieving that change. Other models used in postfire studies, such as the Army Corps of Engineers' HEC-HMS dendritic routing model (e.g. Cydzik & Hogue, 2009) and Fuh's equation (e.g. Wine *et al.*, 2018) are specifically geared towards predicting runoff and do not assess the interaction of processes across the critical zone interface (Maina & Siirila-Woodburn, 2019). Alternatively, many studies have begun to use physically-based distributed models – ParFlow-Community Land Model (CLM; Ashby & Falgout, 1996; Jones & Woodward, 2001; Kollet & Maxwell, 2006; Maxwell, 2013) in particular – to simulate critical zone water and energy transfers and account for the spatial distribution of land surface vegetation in disturbance-affected watersheds (e.g. Atchley *et al.*, 2018; Maina & Siirila-Woodburn, 2019; Mikkelsen *et al.*, 2013; Penn *et al.*, 2016).

In this study, we use the integrated hydrological model ParFlow-CLM with a spatially homogenized domain and set of meteorological forcings to simulate a battery of algorithmically-generated hypothetical fires with specific, predetermined spatial prop-

erties. This approach allows us to explore the fundamental relationships between fire patterns and watershed hydrological processes in an idealized manner by controlling for confounding spatial variables, such as pre-existing ecological landscape patterns and meteorological heterogeneity. The primary objective of this work is to identify when, where, and by how much watershed discharge, ET, soil water storage, and snow dynamics are influenced by changes in postfire spatial patterns alone. We also aim to provide a conceptual understanding of pattern-related interactions between these hydrological variables in such a way as to provide a foundation for future inquiries involving greater complexity.

2.3 Methods

Here we introduce the hydrological model in greater detail (Section 2.2.1); explain the domain configuration and meteorological forcings data (Section 2.2.2); describe the parameterization and validation of burned areas within the domain (Section 2.2.3); and detail a suite of synthetic numerical experiments designed to quantify the impacts of wildfire spatial patterns (Section 2.2.4).

2.3.1 Model Description

ParFlow-CLM is a physically-based, distributed hydrologic model that simulates water and energy fluxes throughout the critical zone – from bedrock to vegetation canopy. ParFlow simultaneously solves the three-dimensional Richards’ equation for subsurface flow and a two-dimensional kinematic wave approximation for surface flow. The CLM module uses vegetation characteristics (leaf area (LAI) and stem area indices (SAI), canopy height, stomatal resistance, etc.) and a time-series of eight spatially distributed atmospheric variables (short- and long-wave radiation, precipitation,

air temperature, east-west and north-south wind speeds, air pressure, and specific humidity) to model land surface processes, such as ET and snow, under a surface energy balance formulation (Kollet & Maxwell, 2008; Maxwell & Miller, 2005). CLM interacts with ParFlow over the ten uppermost soil layers, coupled via a source-sink term in the Richards’ and kinematic wave equations.

2.3.2 Study Domain and Model Setup

We used the CUAHSI CONUS Model Subsetter (Castronova & Tijerina, 2019) to extract a representative watershed from the continental-scale, high-resolution (1 km) PF-CONUS 1.0 dataset (Maxwell *et al.*, 2015; O’Neill *et al.*, 2020), then modified the domain to remove baseline spatial heterogeneity. The subset domain had a total depth of 1 km, which we discretized into 25 layers of variable thicknesses with 980 m of intact bedrock, 19 m of saprolitic granite, and 1 m of soil. No-flow boundary conditions were applied to the sides and to the bottom where the underlying bedrock is assumed impermeable.

While we could have created a purely synthetic domain, this approach generated realistic terrain geometries and allowed us to utilize site-specific, historical meteorological forcings. The subsetter also provided us with vetted land cover and subsurface parameter sets, including: soil hydraulic parameters as described by the soil survey geographic database (SSURGO), deeper geologic units developed from the Gleeson *et al.* (2011) national permeability map, and vegetation classes containing plant functional parameters provided by the International Geosphere-Biosphere Programme (IGBP) database.

We chose the Upper South Fork Salmon River watershed (USFSR) in Central Idaho as our representative watershed. The USFSR was selected for several rea-

sons: (1) its natural homogeneity in terms of geology, soils, and land cover makes it especially suitable for our experimental design; (2) it exists in a region where high-resolution (1 km spatial, hourly temporal) meteorological data was readily available; and (3) as a mountainous, snow-dominated watershed susceptible to wildfire disturbance, it broadly represents a critically important type of watershed (Bladon *et al.*, 2014; Hallema *et al.*, 2018)

The USFSR is approximately 940 km² in size and encompasses the steep, high-elevation headwaters of the South Fork Salmon River. It is located squarely on the Atlanta Lobe of the Idaho Batholith, a granitic pluton that is remarkably uniform in composition and structure (Byerly *et al.*, 2017). As a result, the watershed is blanketed in a consistently shallow, sandy soil that is easily eroded (Arnold & Lundeen, 1968). The USFSR is predominantly covered in evergreen forest with small, scattered pockets of shrubland and grassland (USDA, 2000) and although forest structure and composition varies with elevation, these differences are not distinguished by the IGBP classification system. Ninety-nine percent of the watershed is owned and administered by the US Forest Service, whose primary management goal is the protection of sensitive fish habitats (IDEQ, 2002). As such, while several large wildfires have occurred in the USFSR over the past twenty years, major land disturbing activities like timber harvesting and grazing are fairly limited and urban development is almost nonexistent. Together, these characteristics provide a reasonable basis for assuming landscape uniformity, which was implemented by applying the dominant geologic, soil, and vegetation types to the entire domain.

We chose to run each simulation for the course of one water year to avoid the effects of vegetation regrowth, which is complex and usually starts after the second

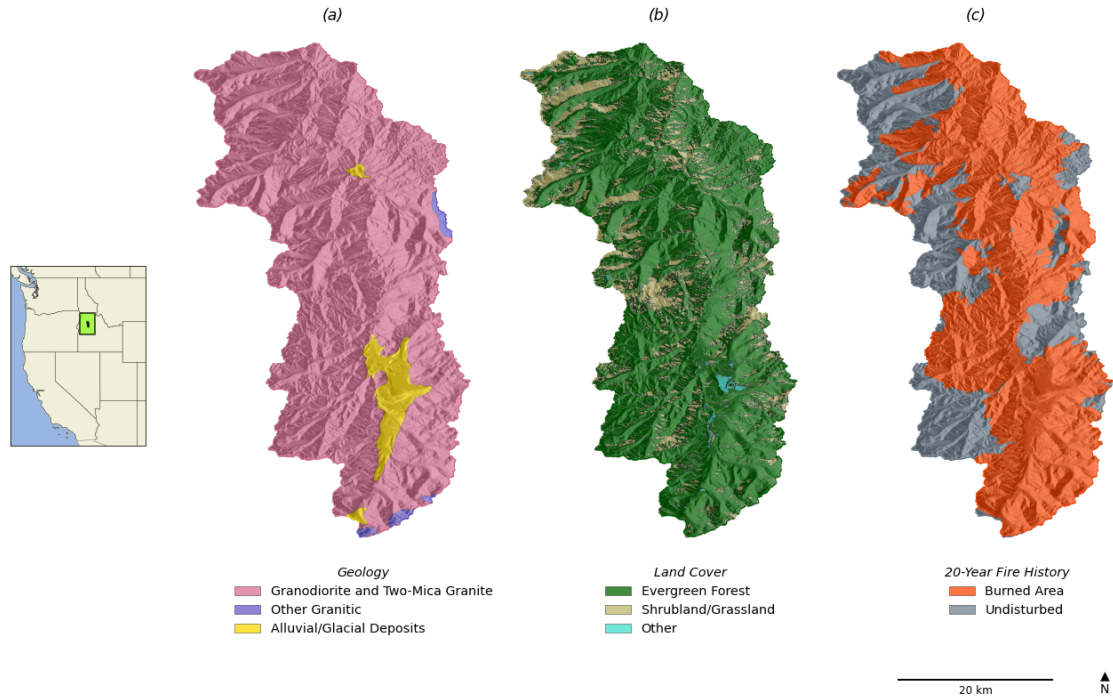


Figure 2.1: Location, (a) geology, (b) land cover, and (c) 20-year fire history of the Upper South Fork Salmon River watershed in central Idaho, U.S.

year of recovery (Kinoshita & Hogue, 2011). We used meteorological data from the 2006 water year as it most closely resembled an average year – the USFSR has a normal mean annual temperature of 2.8°C and receives approximately 1200 mm of precipitation per year on average, falling mostly as snow (IDEQ, 2002). The hourly atmospheric data needed to force the model was obtained from a 30-year climatological dataset generated with the Weather Research and Forecasting (WRF) model by the Lab for Ecohydrology and Applied Forecasting (LEAF) group at Boise State University (Flores *et al.*, 2016). The considerable topographic relief of this watershed (1110 m - 2440 m) results in elevation-dependent spatial heterogeneity in the meteorological variables. This was removed by uniformly assuming the arithmetic mean

value across the domain at each time step, preserving their temporal progressions while allowing us to isolate fire patterns as the only source of spatial heterogeneity in the model domain.

2.3.3 Fire Parameterization

Burned regions were represented in the model by using an additional parameter set that reflects hydrologically-relevant postfire changes to the landscape. For simplicity, all burned areas were identically treated as high severity sites using a representative differenced normalized burn ratio (dNBR) of 897 to set the parameter values discussed below. This value was randomly selected from within the upper 10% of Monitoring Trends in Burn Severity (MTBS) historical burn severity observations from the USFSR over the past 20 years (Eidenshink *et al.*, 2007).

Vegetation Parameters

High severity fire results in widespread vegetation mortality and canopy loss, exposing the surface and reducing biological water demand. Some studies, such as Maina & Siirila-Woodburn (2019), have replaced pre-fire vegetation classes with IGBP “barren soil” parameters as a conservative representation of these land cover changes. Others, like Atchley *et al.* (2018), chose to simply adjust the LAI values in order to represent different burn severities. We used the latter method, reducing the maximum LAI from 6.0 to 0.15 and the minimum LAI from 5.0 to 0.125 (Table 2.1) in accordance with the linear relationship between dNBR and LAI derived from data in Atchley *et al.* (2018).

Table 2.1: Parameter values used to distinguish burned and unburned grid cells in ParFlow-CLM.

| | Unburned | Burned |
|---------------|----------------------|----------------------|
| LAI_{\max} | 6.0 | 0.150 |
| LAI_{\min} | 5.0 | 0.125 |
| K_{st} | 0.0158 | 0.0011 |
| Manning’s n | 4.4×10^{-6} | 2.2×10^{-6} |

Surface-Subsurface Parameters

Wildfire reduces infiltration capacity through the formation of hydrophobic layers and by altering soil hydrodynamic properties like porosity and sorptivity (Hallema *et al.*, 2017). This can be parameterized by decreasing the hydraulic conductivity value, which reasonably approximates the overall effect without needing to explicitly represent each individual mechanism (Atchley *et al.*, 2018; Ebel & Martin, 2017; Maina & Siirila-Woodburn, 2019; Moody *et al.*, 2013). We used the relationship between dNBR and hydraulic conductivity provided by Moody *et al.* (2015) to estimate an appropriate high soil burn severity value (Table 2.1). In order to carry out the calculation, we used our representative dNBR and adjusted the unitless coefficient to fit the pre-fire hydraulic conductivity as was done in Atchley *et al.* (2018):

$$K_{st} = 167 \exp(-0.0056 \text{ dNBR}) \quad (2.1)$$

The destruction of litter, duff, and understory vegetation is thought to accelerate runoff by decreasing surface roughness (Johansen *et al.*, 2001; Larsen *et al.*, 2009; Lavee *et al.*, 1995). Although its relative contribution to observed increases in postfire runoff is not well understood (Larsen *et al.*, 2009; Shakesby *et al.*, 2000), it appears to serve an important role in runoff routing (Reaney *et al.*, 2014). Because postfire

surface roughness is rarely determined quantitatively (Lavee *et al.*, 1995), we roughly estimated a 50% reduction in the Manning’s n value (Table 2.1).

The synthetic nature of the numerical experiments designed and conducted here means that there are no datasets that afford a rigorous validation of model outputs that compare burned and unburned conditions under similar climate forcings. Specifically, the scenarios of both the fraction and spatial configuration of burned areas in the USFSR have never been, and likely never will be, fully realized in a way that would represent something like a controlled experiment in nature. Thus, a heuristic analysis of model outputs under both burned and unburned conditions is necessary to provide reasonable confirmation for our parameterization of fire effects on soils and vegetation. Here we are interested in the extent to which our burned scenarios – when compared with unburned scenarios under similar conditions – reproduce the direction of change in a number of key hydrologic states and fluxes (e.g., discharge, soil moisture, evapotranspiration, and snow water equivalent) that are reported in the literature for forested, snow-dominated mountain watersheds. To this end, we ran and compared two baseline control simulations: one where no fire was represented and another where the entire watershed was burned. We found a general agreement between this comparison and what is currently understood about post-fire hydrology, suggesting that our parameterization is a reasonable representation of burned sites.

2.3.4 Generating Postfire Landscapes

To investigate the link between wildfire patterns and hydrological processes, we developed a suite of stochastically generated postfire landscapes that arrange our two distinct classes (burned, unburned) into mosaics representing different characteristic patterns. Each landscape is a two-dimensional grid identical to the model domain,

with exactly 200/897 grid cells classified as burned – the only difference being the arrangement of burned cells within the landscape.

We created the mosaics using neutral landscape models as implemented by the Python package NLMpy (Etherington *et al.*, 2015). NLMpy contains several mapping algorithms that produce arrays of values between 0 and 1 by manipulating the spatial autocorrelation in different ways. We created three groups of 50 landscapes using random (group R), random cluster nearest-neighbor (group NN), and midpoint displacement (group MPD) algorithms (Fig. 2.2).

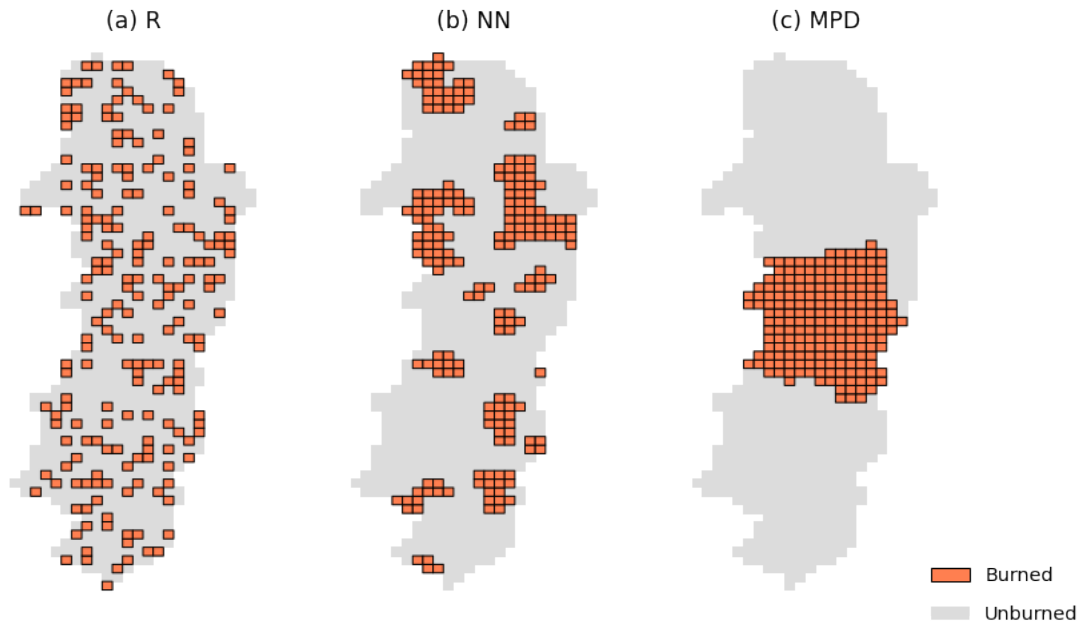


Figure 2.2: Examples of the postfire landscapes generated by (a) random, (b) random cluster nearest-neighbor, and (c) midpoint displacement algorithms.

As the name suggests, the random algorithm independently assigns values from a random distribution (Palmer, 1992), resulting in maximum disaggregation and very little connectivity (Fig. 2.2a). The midpoint displacement algorithm – an approxima-

tion of fractional Brownian motion (Fournier *et al.*, 1982) – allows for explicit control over spatial autocorrelation. We maximized the spatial autocorrelation parameter in this algorithm to generate landscapes containing a single, large patch of burned cells (Fig. 2.2c). Finally, the random cluster nearest-neighbor algorithm adopted from Saura & Martínez-Millán (2000) was used to produce postfire landscapes intermediate to the endmembers previously discussed, consisting of approximately 15 variably sized clusters of burned cells that are randomly distributed and disconnected from one another (Fig. 2.2b).

Each algorithm produces a characteristically different pattern, which we quantified using the landscape metric contagion. The contagion index is a measure of aggregation that reflects the probability that two randomly selected adjacent elements are of the same class:

$$CONTAG = 1 + \frac{\sum_{i=1}^m \sum_{k=1}^m \left[P_i \frac{g_{i,k}}{\sum_{k=1}^m g_{i,k}} \right] \left[\ln \left(P_i \frac{g_{i,k}}{\sum_{k=1}^m g_{i,k}} \right) \right]}{2 \ln(m)} \quad (2.2)$$

where P_i is the proportion of the landscape occupied by elements of class i , $g_{i,k}$ is the number of adjacencies between i and k classes, and m is the number of classes present in the landscape (McGarigal, 2015). Contagion does not attempt to measure hydrologic connectivity, rather it is a process-neutral way of numerically describing the difference between our groups in terms of pattern alone. We used the PyLandStats Python package (Bosch, 2019) to calculate contagion values for each experimental landscape, which are summarized in (Table 2.2).

Each hypothetical mosaic was mapped to the model domain and simulated over the course of one water year. With all but the arrangement of cells held constant, any

variation between the simulations should be attributable to differences in pattern.

Table 2.2: Mean (SD) contagion values for each experiment group.

| Group | Contagion |
|-------|-------------------|
| R | 0.228 ± 0.004 |
| NN | 0.336 ± 0.003 |
| MPD | 0.504 ± 0.003 |

2.4 Results

In this section, we examine the timing and relative magnitude of variation between simulations for each water balance term. We then identify relationships between different hydrologic processes and how they are correlated with measures of landscape aggregation and connectivity.

2.4.1 Controls and Null Predictions

The only difference between experimental simulations is the arrangement of burned and unburned grid cells. ParFlow-CLM is a deterministic model, meaning identical initial conditions will produce identical outcomes — so under the null hypothesis that pattern has no hydrologic influence, each grid cell would operate independently according to its assigned parameters and thus the domain-wide results would be identical across the suite of mosaics. Furthermore, we can compute a null prediction at each time step using a simple endmember mixing model:

$$X_{\text{predicted}_t} = \alpha X_{\text{unburned}_t} + \beta X_{\text{burned}_t} \quad (2.3)$$

where X is the model output for a given variable at time t , α is the proportion of unburned cells in the experiment domain, and β is the proportion of burned cells in

the experiment domain.

Figure 2.3 shows watershed-averaged accumulated discharge, change in soil water storage relative to the initial conditions, snow water equivalent (SWE), and evapotranspiration (ET) throughout the water year for the 100% burned and unburned control simulations, null predictions, and range of experimental results.

The rate of snow accumulation was slightly higher in the burned control than in the unburned control, yet SWE was kept more or less equivalent through much of the winter by unseasonably warm melt events in November and December that predominantly affected the burned landscape. In the 100% burned case, peak SWE occurred two weeks earlier and was approximately 35 mm lower than in the unburned control case. This contrasts with Maina & Siirila-Woodburn (2019) whose ParFlow-CLM modeling study in the Sierra Nevadas found that peak SWE was higher in post-fire simulations compared to pre-fire simulations with no offset in timing. However, SWE was 3% greater in our burned control case at the time it reached peak SWE and the unburned control had an overall higher peak SWE due to continued accumulation as the burned control began melting. In addition to earlier melt onset, snow also melted more rapidly in the burned control, reaching the snow disappearance date 4 weeks sooner than in the unburned case. This is consistent with Uecker *et al.* (2020) which found that a shift in postfire snowmelt timing in the Washington Cascades led to snow disappearing on average 19 ± 9 days earlier compared to pre-fire conditions.

Snowmelt was the primary driver of runoff generation in both control simulations. Total annual discharge was approximately 240 mm higher in the 100% burned scenario than in the unburned control and concluded one month earlier, coinciding with the end of the snowmelt period. Despite reduced hydraulic conductivity, soil water storage

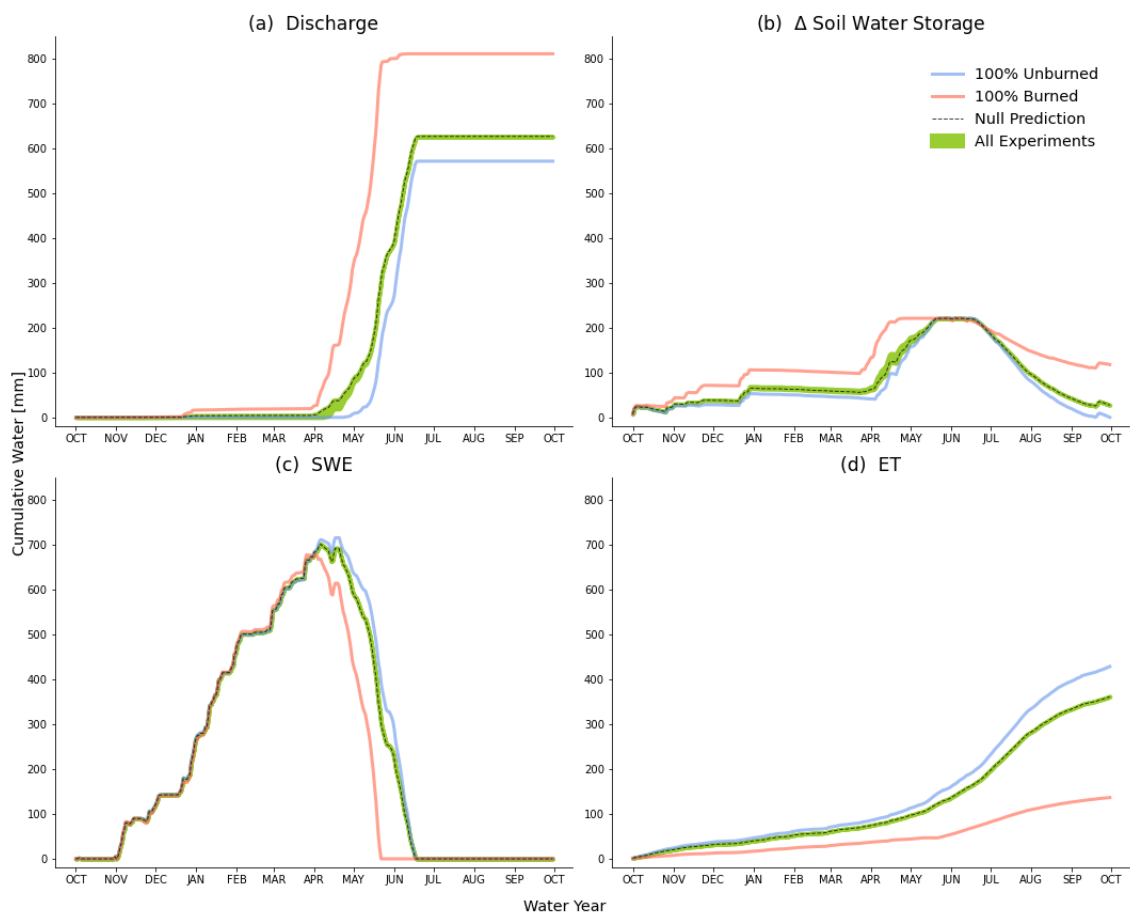


Figure 2.3: Comparison of watershed-averaged cumulative (a) discharge, (b) change in soil water storage relative to initial conditions, (c) snow water equivalent (SWE), and (d) evapotranspiration (ET) between the two control endmembers: burned (red) and unburned (blue), the null prediction (dotted line), and range of experimental results (green).

was consistently greater in the 100% burned scenario relative to the unburned control. In either case, soil water storage reached a maximum shortly after the onset of the melt season once the soil was completely saturated, then began to decrease as water was drawn from the soil to support ET. As expected, ET was much lower (300 mm) in the 100% burned scenario compared to the unburned control due to an absence of healthy vegetation. Consequently and similar to the findings in Cardenas & Kanarek (2014), soil moisture was more quickly depleted in the unburned watershed, resulting

in approximately 120 mm more water stored in the burned soils by the end of the water year.

2.4.2 Variation in Experimental Simulations

The experimental simulations closely followed the null prediction line for each of these processes, with the standard deviation of their annual totals all less than 0.5 mm. This suggests that fire size and/or severity have a much greater influence on postfire hydrologic outcomes than spatial patterns. On the other hand, one-way ANOVA differences between groups for all four variables were statistically significant ($p \ll 0.05$) at every eligible time step save the first few weeks. While SWE and accumulated ET showed relatively small but significant variation throughout the water year, accumulated discharge and change in soil water storage temporarily varied by as much as 20 mm during the spring months (April to June). This is an order of magnitude higher than anywhere else, indicating the presence of important pattern-related interactions in these periods.

Figure 2.4 shows biweekly totals for each hydrologic process relative to their null predictions. Each marker represents the watershed-averaged value for an individual experiment with color corresponding to the contagion group to which it belongs. Recall that R (green) possesses the least aggregated burned grid cells, MPD (blue) is the most aggregated, and NN (orange) is intermediate. Around the beginning of January and in early to mid April, less aggregated fires had systematically lower discharge while also exhibiting systematically greater increases in soil water content. The pattern inverted from late April through May but the relationship between soil moisture and discharge was preserved (i.e., a positive departure in discharge was associated with a negative departure in soil water storage and vice versa).

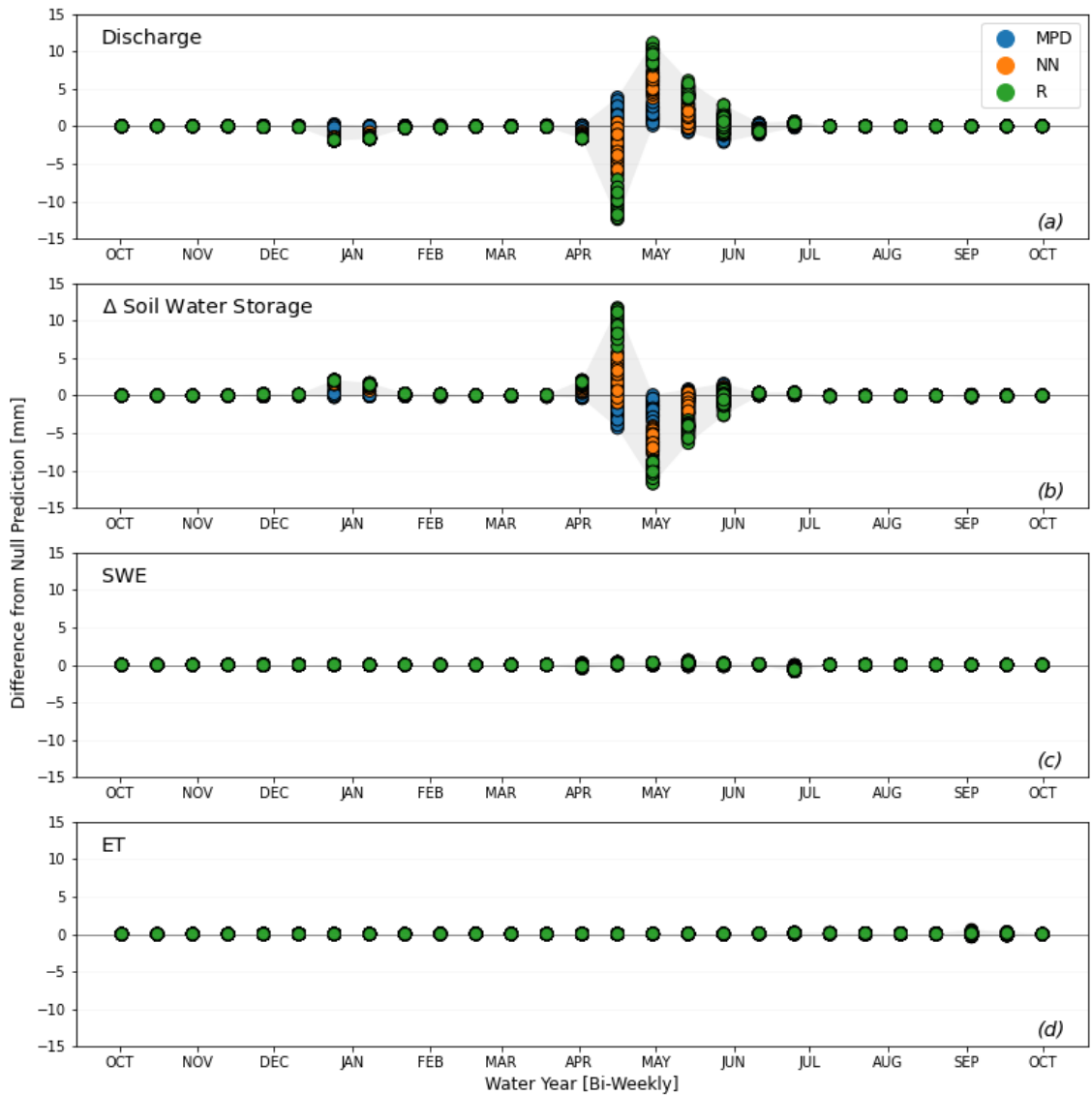


Figure 2.4: Biweekly total (a) discharge, (b) change in soil water storage, (c) snow water equivalent (SWE), and (d) evapotranspiration (ET) for each simulation. Color indicates group membership with green being the least aggregated, blue the most aggregated and orange intermediate.

The evolution of discharge and soil moisture variation between experiments was associated with differences in snowmelt timing between burned and unburned grid cells. In each simulation, the timing of peak SWE and the date of snow disappearance

for burned and unburned grid cells matched the timing of their respective control simulations. Figure 2.5 compares each variable's time series of year-to-date standard deviations across all experiments with peak SWE and snow-free dates for burned and unburned areas as well as the timing of accumulation season snowmelt events. Discharge is flipped about the y-axis to highlight its relationship with soil water storage.

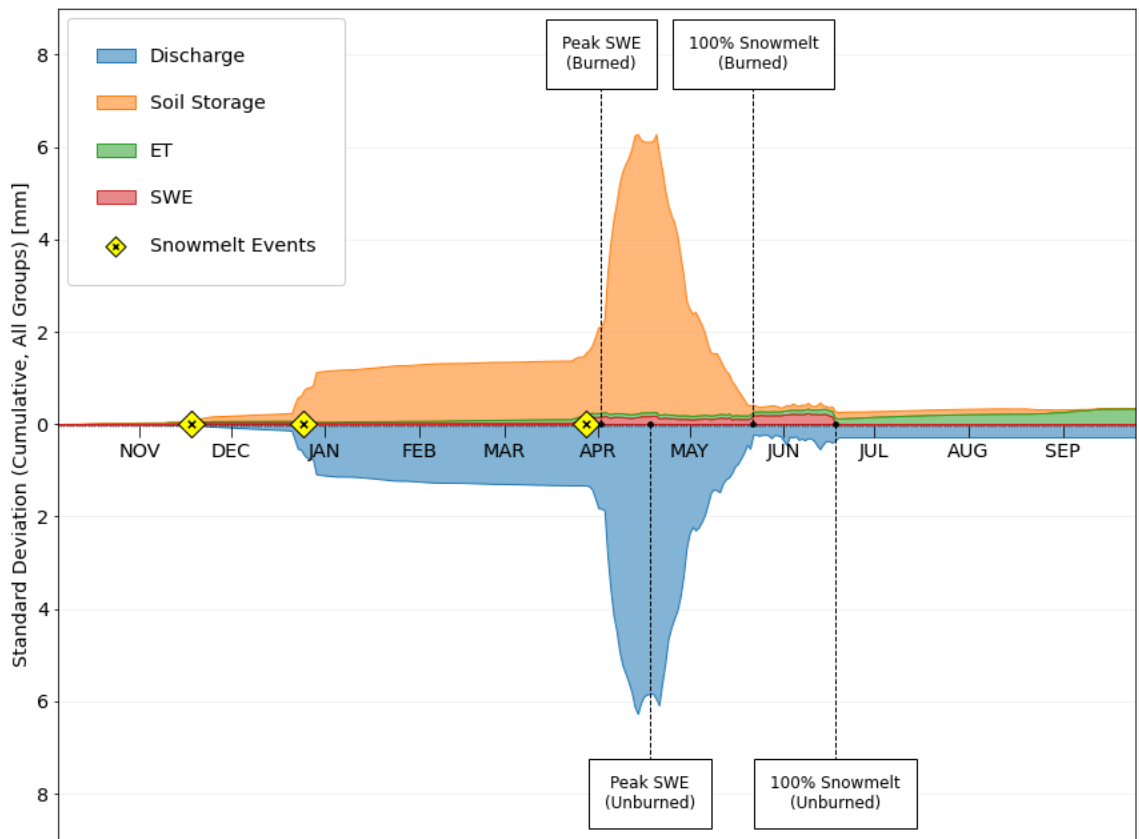


Figure 2.5: Timeseries of year-to-date standard deviations between all experiments for discharge, soil water storage, evapotranspiration (ET), and snow water equivalent (SWE). Discharge (blue) is flipped about the y-axis to highlight its relationship with soil water storage and markers indicate snowmelt events and benchmarks that correlate with changes in variability.

The snowmelt events (each preferentially melting burned areas) corresponded with

sudden, short-term increases in standard deviation for both discharge and soil storage and a sustained, rapid increase in variation occurred once the burned areas reached peak SWE at the beginning of April. Maximum variation occurred around the time unburned areas started melting. Immediately thereafter, the standard deviation between experiments collapsed, stabilizing at values below 0.5 mm by the time the burned areas were completely melted.

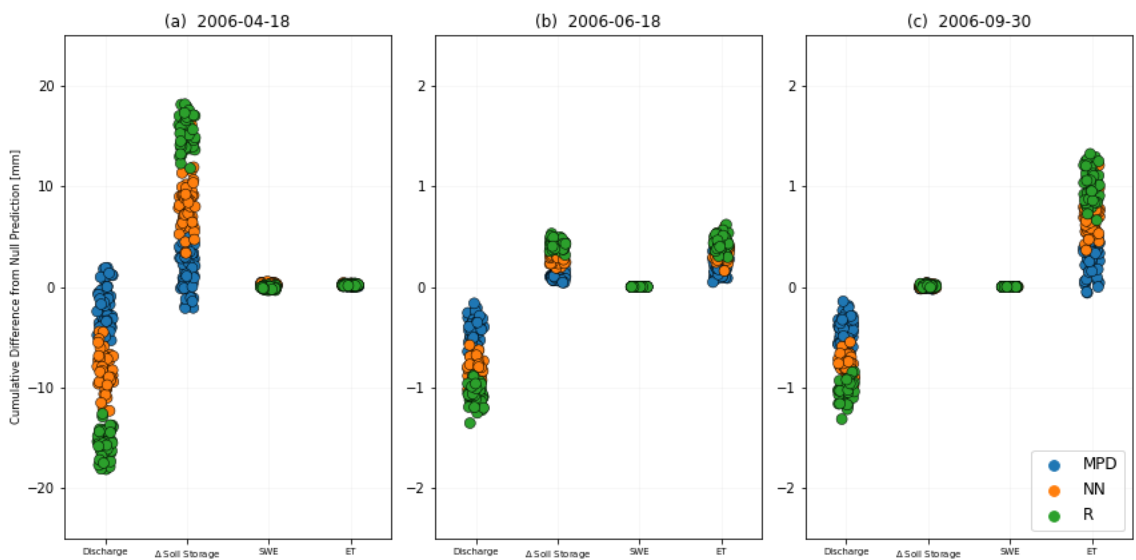


Figure 2.6: Accumulated discharge, change in soil water storage, snow water equivalent (SWE), and evapotranspiration (ET) of each experiment at (a) peak SWE in unburned areas, (b) the snow disappearance date in all areas, and (c) the end of the water year. Color indicates group membership with green being the least aggregated, blue the most aggregated and orange intermediate.

Meanwhile, differences in soil moisture between the experiments were linked to the rate of ET. Figure 2.6 illustrates how the variation in soil water storage was transferred into variation in ET. Each marker represents the year-to-date total of an individual experiment relative to the null prediction, with color denoting group membership. When the unburned areas reached peak SWE (Fig. 2.6a), the variation in discharge and soil storage was at a maximum, directly offsetting each other. The

least aggregated group R experiments were the farthest from the null prediction regardless of sign, whereas the most aggregated group MPD experiments showed the least departure. Once all the snow had melted (Fig. 2.6b), the remaining variation in discharge was balanced by an even split between soil moisture and ET with the relationship between experimental groups preserved. While no further changes in discharge were recorded through to the end of the water year (Fig. 2.6c), all of the variation in soil water storage was gradually ceded to ET.

2.4.3 Aggregation and Connectivity

As demonstrated, the interaction between discharge and soil water storage — and consequently between soil water and ET — is associated with the level of fire aggregation, or contagion. However, there is substantial intra-group variation despite the experimental mosaics in each group having identical measures of contagion. This is explained by the fact that while watershed-averaged variation is increasing at times when only burned areas are melting, differences between simulations actually occur in downgradient, hydrologically connected unburned areas.

Figure 2.7 demonstrates the relationship between year-to-date watershed-averaged discharge and soil water storage relative to the null prediction, and the number of unburned grid cells contained in flow paths between burned areas and the watershed outlet at the time of maximum variation (April 18). Each marker indicates an individual model run with an alternative realization of fire for land cover with color indicating the total number of unburned grid cells along the burned flow paths. Discharge and soil water storage show a negative linear relationship, which is itself correlated with total unburned area hydrologically downslope of the fire.

The side panels (Fig. 2.7b - 2.7e) show examples of fire mosaics with different

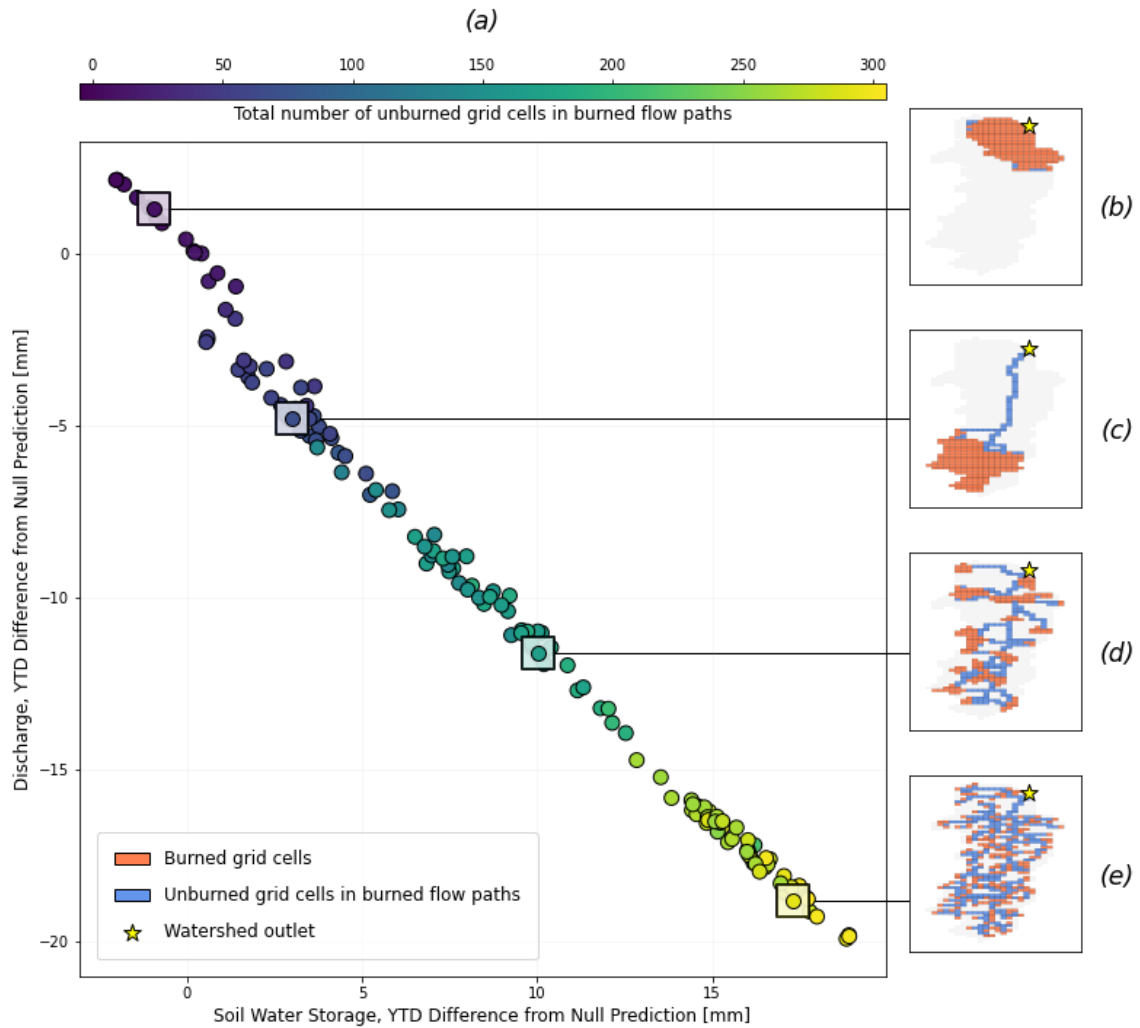


Figure 2.7: (a) Correlation between year-to-date discharge and soil water storage relative to their null predictions at the time of maximum variation. Color indicates the total number of unburned grid cells in the disturbance flow network. Simulations with fewer unburned grid cells in the disturbance flow network have greater discharge and lower soil water storage. (b - e) Disturbance flow network maps corresponding to specific experiments, illustrating the differences in unburned grid cells.

flow path lengths. Here, the blue grid cells represent unburned areas that are directly downstream of burned areas and thus hydrologically connected to the burned areas (red grid cells). Although they are not directly impacted by wildfire, these areas may be indirectly affected by runoff generated in or flowing through the burn scars. For

that reason and for the sake of brevity, in the results and discussion that follows that we refer to these as the unburned component of fire disturbance flow path network.

2.5 Discussion

2.5.1 Disturbance Flow Path Networks

Throughout the watershed, runoff was exclusively generated by snowmelt due to low antecedent soil moisture and a paucity of rainfall events during the 2006 water year. Since each burned grid cell accumulated the same amount of SWE regardless of pattern, the amount of runoff generated within the fire was essentially identical across experiments. It was the infiltration capacity gradient between burned and unburned grid cells that caused all significant deviations from the endmember mixing models (null predictions). As the surface runoff flowed out the burned area, the higher surface roughness and greater hydraulic conductivity of the unburned grid cells slowed and pulled more water into the soil than would have happened otherwise.

Each experimental representation of fire created a different network of disturbance flow paths composed of burned and hydrologically connected unburned sites. Although the number of burned grid cells was held constant, the unburned component of the disturbance flow path network ranged from 0 - 50% of all unburned grid cells, depending on the spatial arrangement of burned sites. Thus, differences between experiments arose because more and more of the runoff was infiltrated as it flowed through additional unburned grid cells, ultimately influencing both soil water storage and the amount of discharge at the watershed outlet. Furthermore, earlier wetter soils in these connected, unburned areas marginally increased ET compared to unconnected unburned sites and, consequently, the watershed-averaged total annual

ET was also associated with the number of unburned grid cells in the disturbance flow path network.

In general, highly aggregated fires created shorter paths through unburned territory because runoff was consolidated prior to leaving the burned area. However, depending on the fire's distance from the watershed outlet and the degree to which patches straddled catchment divides, the length of the disturbance flow path network could vary significantly even amongst equally aggregated fires. For example, Figure 2.8 shows two samples from the NN group where despite nearly indistinguishable levels of aggregation (difference in contagion: 0.002), the unburned portion of the disturbance flow network differs by nearly a factor of two. Because of the importance of these indirectly affected unburned areas, attempts to quantify postfire spatial patterns in watershed-scale hydrological contexts should include the entirety of the disturbance flow path network rather than just the fire boundaries and unburned patches within. This supports the findings of Moody *et al.* (2008), which showed that observed rainfall-discharge relationships in the 2000 Cerro Grande Fire near Los Alamos, NM were a linear function of hydraulic functional connectivity, a metric incorporating spatial sequences of different burn severity magnitudes along hillslope flow paths. We expect that such a metric could also be used to predict postfire soil moisture and evapotranspiration as well.

One limitation of the ParFlow-CLM model is that it does not explicitly represent stream channels. On one hand, this is advantageous in that by using pressure heads and terrain geometry for overland flow routing, the process is physically-based and mass conserving. On the other hand, surface water is assumed to be uniformly distributed across each grid cell. This assumption is particularly problematic at a

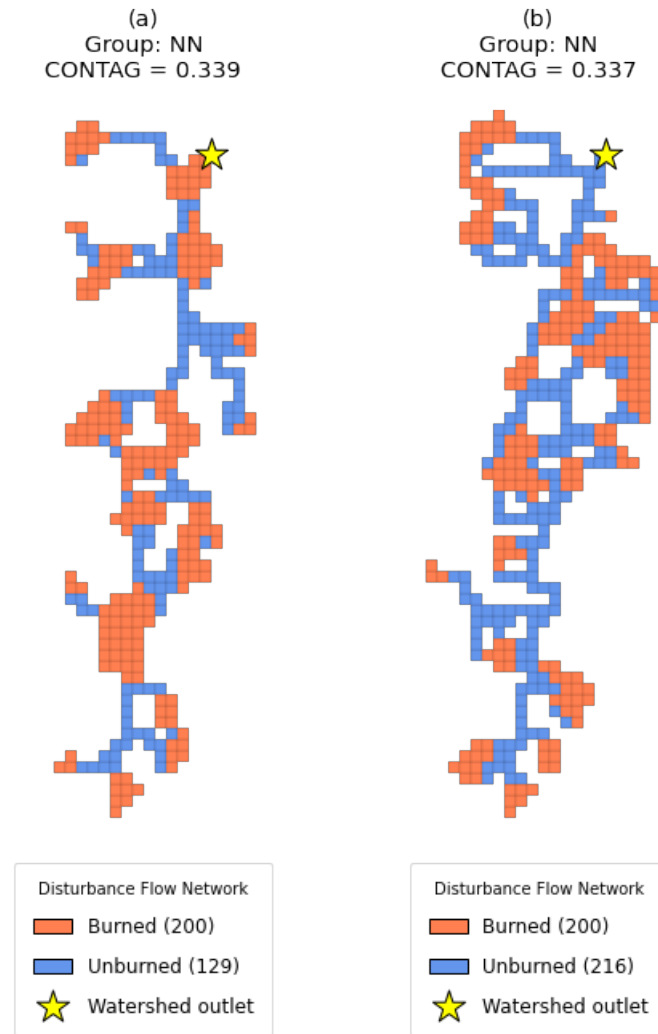


Figure 2.8: Comparison of disturbance flow path networks between two post-fire landscapes generated with the random cluster nearest-neighbor algorithm with similar contagion values. While both have the same number of burned grid cells, (a) has significantly fewer hydrologically connected unburned grid cells than (b).

spatial resolution of 1 km, likely significantly increasing the infiltration potential of each grid cell. Grid cells with greater contributing areas may have inflated infiltration rates compared to those with smaller contributing areas, resulting in underestimated discharge for highly aggregated fires and overestimated discharge for highly disaggregated fires. This suggests that the observed differences between spatial patterns may

be somewhat conservative. On the other hand, by using a single, high burn severity parameterization we maximized the infiltration capacity gradient between burned and unburned grid cells, potentially exaggerating the effects of postfire spatial patterns. It is likely that these competing sources of uncertainty are occurring simultaneously and it is difficult to know whether they balance or if one has a stronger impact than the other. While the variation between experiments was statistically and systemically significant, the departure from the null prediction was already relatively small compared to the difference between the null prediction and the prefire control simulation. If the effects are indeed exaggerated, it suggests that fire size and severity are much more important controls on postfire hydrologic processes than pattern. Even if our results are conservative, it is unlikely that connectivity is the more important factor as proposed by Cawson *et al.* (2013) in their experiments with prescribed burns.

2.5.2 Snow-dominated Mountain Watersheds

Most prior studies examining the hydrologic impacts of postfire spatial patterns have focused on individual rainfall events, finding pattern-related differences in runoff magnitude. Our study primarily considered spatial patterns from the perspective of snowmelt-driven runoff. The spatial relationships between burned and unburned (or between various burn severity magnitudes) is a controlling factor in runoff response in either case. However, snowmelt processes introduce additional layers of complexity that ultimately influence runoff timing more so than magnitude. Pattern-related effects are particularly pronounced at the very beginning of the snowmelt season when the infiltration capacity gradient is rather large and burned areas are producing runoff capable of leveraging that gradient. As the soil in the unburned portion of the disturbance flow path network approaches saturation, the gradient disappears and the

maximum possible divergence between different spatial patterns is reached. Up until this point in all of our simulations, snow was melting in the burned areas but not in the unburned areas; but as soon as the unburned areas begin melting, meltwater that otherwise would have infiltrated into the unburned portion of the disturbance flow path network (now fully saturated) is committed to discharge instead, making up for the previous deficit. This can be seen in Figure 2.4 with the sudden pattern inversion and in Figure 2.5 where the total year-to-date variability between experiments collapses, both occurring at the same time in late April. As a result, total annual discharge and year-end soil water storage values are virtually identical regardless of postfire spatial patterns.

The infiltration capacity gradient is made possible through differences in hydraulic conductivity and surface roughness between burned and unburned sites. The disturbance flow path network – arising from the spatial arrangement of burned grid cells – controls the degree to which that gradient affects watershed-scale processes. However, it is the timing difference in snowmelt onset (burned before unburned) that leverages the gradient, driving the interactions we see. There are many factors governing snow dynamics, many of which are ignored in our attempt to control for postfire spatial patterns by homogenizing the meteorological forcings. Regardless, it is important to consider whether these snowmelt behaviors are reasonable. Without a timing difference, the infiltration capacity gradient likely closes too quickly to have a substantial effect. If unburned snowmelt precedes burned snowmelt, similar interactions might occur but perhaps within the postfire areas rather than downstream.

Maina & Siirila-Woodburn (2019) is particularly interesting in this regard because they found no difference in snowmelt timing despite using the same modeling

platform (ParFlow-CLM). Snow processes are handled by the CLM module and we chose to represent burned areas within CLM by reducing the LAI as was done in Atchley *et al.* (2018). This leaves the SAI and related reflectance values unchanged from those of the prefire vegetation. Maina & Siirila-Woodburn (2019), on the other hand, used a more traditional “barren soil” representation that eliminates all traces of vegetation. Reduced forest density, as is likely in severely burned areas, has been shown to reduce snowmelt rates because longwave radiation emanating from overstory vegetation outweighs the increase in shortwave radiation from loss of canopy cover (Dickerson-Lange *et al.*, 2015; Lundquist *et al.*, 2013). It is possible that the “barren soil” parameterization reproduces this effect while our approach where SAI is left intact does not. Studies have also shown that the inclusion of black carbon from partially combusted organic material reduces the albedo of postfire snowpacks, causing the rate of snowmelt to increase (Gleason *et al.*, 2013; Uecker *et al.*, 2020). Although there is currently no way to control snowpack albedo in ParFlow-CLM, this suggests that our results may nevertheless realistically represent postfire snow dynamics.

Insofar as snowmelt-driven hydrological processes are concerned, as long as accumulated SWE is greater than the watershed soil storage capacity postfire connectivity should not have a considerable effect on the total annual quantity of water balance terms, only in timing. However, as seasonal snowpack continues to decline in the western United States due to rising temperatures (Mote *et al.*, 2018), years where SWE is less than the soil storage capacity will undoubtedly become more common. In these cases, postfire spatial patterns could have a marked effect, especially with regard to annual discharge and ET.

2.5.3 Recommended Future Work

Our objectives for this work were twofold: (1) identify how changes in postfire spatial patterns fundamentally influence hydrological interactions within the watershed, and (2) provide a methodological and conceptual foundation for future inquiries to build upon. With respect to the latter, here we recommend three broad areas for continuing this work.

a. Changing the meteorological conditions

Our results suggest that a wildfire's spatial pattern primarily impacts the timing of watershed discharge and downstream soil moisture due to differences in snowmelt onset and infiltration capacity between burned and unburned sites. However, it is difficult to generalize our findings because we chose to use only a single set of forcings. This leaves a number of questions unanswered that could be addressed simply by using different forcings with specific, desired characteristics. For example, what are the consequences if snowmelt onset differences are reversed or nonexistent? What happens if total SWE is less than the soil storage capacity and the watershed does not become fully saturated?

b. Restoring competing sources of heterogeneity

A consequence of controlling for competing sources of heterogeneity in order to isolate the influence of postfire spatial patterns is that our results have limited applicability toward actual fire-disturbed watersheds. By incrementally adding back those spatial complexities (i.e. meteorological forcings, vegetation distribution, etc.), we may be able to track the original pattern-related signal to determine its relative strength in comparison. As this work continues, we

will approach a realistic watershed representation and gain a more nuanced understanding of the hydrological influences of wildfire spatial patterns.

c. Quantifying the disturbance network

While landscape ecology has provided a number of metrics for quantifying spatial patterns, none were developed from a hydrological perspective. We elected to use the contagion metric under the assumption that measures of aggregation would be a suitable proxy for postfire hydrologic connectivity. However, even with all of our simplifications, we found considerable variation in hydrologic responses between fires with essentially identical contagion. The problem is that contagion measures the spatial relationships between members of the same class, yet we found that the characteristics of the entire disturbance flow path network (containing both burned and unburned sites) was critically important. This necessitates the development of new metrics for quantifying wildfire spatial patterns, an example being functional hydraulic connectivity from Moody *et al.* (2008). Our methodology could be useful for developing and testing spatial metrics like these, especially if done in parallel with incrementally restoring competing sources of heterogeneity.

2.6 Conclusion

As high-elevation forests become increasingly susceptible to severe wildfire disturbances, understanding the factors governing postfire hydrology at the watershed level is crucial for effectively managing water resources. In this work, the coupled surface-subsurface hydrologic model, ParFlow-CLM, was used to investigate how wildfire spatial patterns influence the timing and magnitude of various hydrological processes

in a snow-dominated, mountain watershed. Using a simplified representative watershed and spatially uniform meteorological forcings to control for confounding heterogeneities, 150 variably patterned postfire landscapes were simulated over the course of a single water year. The results indicate the following:

- Wildfire pattern primarily affects the timing of watershed discharge and soil water storage through an infiltration gradient between burned and unburned sites. There was little difference in total annual quantities by the end of the water year due to accumulated SWE being greater than the soil storage capacity. However, because some patterns saw wetter soils earlier in the year, total annual ET was marginally higher at the expense of total annual discharge.
- The size of the unburned component of a fire's disturbance flow path network (comprising all hydrologically-connected burned and unburned sites) is directly associated with discharge and soil moisture timing. In our experiments, cumulative discharge was delayed in mosaics with larger networks due to increased infiltration as runoff from burned areas travelled greater distances through unburned terrain. The disturbance flow path network was determined by the fire's level of aggregation and position relative to subcatchment divides and the watershed outlet.
- The difference in snowmelt onset timing between burned (earlier) and unburned (later) areas drove the observed interactions by creating runoff capable of leveraging the infiltration gradient. If snowmelt had occurred simultaneously, the gradient may not have existed at all and there may not have been any discernible differences between simulations.

This analysis has allowed us to identify where, when, and between which water balance components wildfire spatial patterns have the most impact. It also highlights the importance of hydrologically connected undisturbed areas outside the fire boundary. However, future work in which layers of complexity are incrementally restored to the model is needed to fully understand the role of postfire spatial patterns, particularly in the context of competing meteorological, topographical, and ecological heterogeneity.

References

- Andréassian, Vazken, Lerat, Julien, Le Moine, Nicolas, & Perrin, Charles. 2012. Neighbors: Nature's own hydrological models. *Journal of Hydrology*, **414-415**(Jan.), 49–58.
- Arnold, John F, & Lundeen, Lloyd J. 1968. South Fork Salmon River special survey, soils and hydrology. *Boise, ID: US Department of Agriculture, Forest Service, Boise National Forest*.
- Ashby, Steven F, & Falgout, Robert D. 1996. A parallel multigrid preconditioned conjugate gradient algorithm for groundwater flow simulations. *Nuclear science and engineering*, **124**(1), 145–159. Publisher: Taylor & Francis.
- Atchley, Adam L, Kinoshita, Alicia M, Lopez, Sonya R, Trader, Laura, & Middleton, Richard. 2018. Simulating surface and subsurface water balance changes due to burn severity. *Vadose Zone Journal*, **17**(LA-UR-18-26917). Publisher: Los Alamos National Lab.(LANL), Los Alamos, NM (United States).
- Benavides-Solorio, Juan, & MacDonald, Lee H. 2001. Post-fire runoff and erosion from simulated rainfall on small plots, Colorado Front Range. *Hydrological Processes*, **15**(15), 2931–2952.
- Bladon, Kevin D, Emelko, Monica B, Silins, Uldis, & Stone, Micheal. 2014. *Wildfire and the future of water supply*.
- Bosch, Martí. 2019. PyLandStats: An open-source Pythonic library to compute

- landscape metrics. *PloS one*, **14**(12), e0225734. Publisher: Public Library of Science San Francisco, CA USA.
- Burles, Katie, & Boon, Sarah. 2011. Snowmelt energy balance in a burned forest plot, Crowsnest Pass, Alberta, Canada. *Hydrological Processes*, n/a–n/a.
- Byerly, A, Tikoff, B, Kahn, M, Jicha, B, Gaschnig, R, & Fayon, AK. 2017. Internal fabrics of the Idaho batholith, USA. *Lithosphere*, **9**(2), 283–298. Publisher: Geological Society of America.
- Cannon, Susan H, Gartner, JE, Parrett, Charles, & Parise, Mario. 2003. Wildfire-related debris-flow generation through episodic progressive sediment-bulking processes, western USA. *Debris-Flow Hazards Mitigation: Mechanics, Prediction, and Assessment*. Millpress, Rotterdam, 71–82.
- Cardenas, M Bayani, & Kanarek, Michael R. 2014. Soil moisture variation and dynamics across a wildfire burn boundary in a loblolly pine (*Pinus taeda*) forest. *Journal of hydrology*, **519**, 490–502. Publisher: Elsevier.
- Castronova, Tony, & Tijerina, Danielle. 2019 (July). *CUAHSI/nwm_subsetting: CUAHSI Subsetter*.
- Cawson, JG, Sheridan, GJ, Smith, HG, & Lane, PNJ. 2013. Effects of fire severity and burn patchiness on hillslope-scale surface runoff, erosion and hydrologic connectivity in a prescribed burn. *Forest Ecology and Management*, **310**, 219–233. Publisher: Elsevier.
- Certini, Giacomo. 2005. Effects of fire on properties of forest soils: a review. *Oecologia*, **143**(1), 1–10.

- Collins, Brandon M., Fry, Danny L., Lydersen, Jamie M., Everett, Richard, & Stephens, Scott L. 2017. Impacts of different land management histories on forest change. *Ecological Applications*, **27**(8), 2475–2486.
- Cydzik, Kristina, & Hogue, Terri S. 2009. Modeling Postfire Response and Recovery using the Hydrologic Engineering Center Hydrologic Modeling System (HEC-HMS). *JAWRA Journal of the American Water Resources Association*, **45**(3), 702–714.
- Dennison, Philip E., Brewer, Simon C., Arnold, James D., & Moritz, Max A. 2014. Large wildfire trends in the western United States, 1984-2011: DENNISON ET. AL.; LARGE WILDFIRE TRENDS IN THE WESTERN US. *Geophysical Research Letters*, **41**(8), 2928–2933.
- Dickerson-Lange, Susan E, Lutz, James A, Martin, Kael A, Raleigh, Mark S, Gersonde, Rolf, & Lundquist, Jessica D. 2015. Evaluating observational methods to quantify snow duration under diverse forest canopies. *Water Resources Research*, **51**(2), 1203–1224. Publisher: Wiley Online Library.
- Ebel, Brian A, & Martin, Deborah A. 2017. Meta-analysis of field-saturated hydraulic conductivity recovery following wildland fire: Applications for hydrologic model parameterization and resilience assessment. *Hydrological Processes*, **31**(21), 3682–3696. Publisher: Wiley Online Library.
- Eidenshink, Jeff, Schwind, Brian, Brewer, Ken, Zhu, Zhi-Liang, Quayle, Brad, & Howard, Stephen. 2007. A Project for Monitoring Trends in Burn Severity. *Fire Ecology*, **3**(1), 3–21.

- Etherington, Thomas R, Holland, E Penelope, & O'Sullivan, David. 2015. NLM py: a python software package for the creation of neutral landscape models within a general numerical framework. *Methods in Ecology and Evolution*, **6**(2), 164–168. Publisher: Wiley Online Library.
- Flores, Alejandro, Masarik, Matt, & Watson, Katelyn. 2016. *30-Year, Multi-Domain High-Resolution Climate Simulation Dataset for the Interior Pacific Northwest and Southern Idaho [Data set]*.
- Fournier, Alain, Fussell, Don, & Carpenter, Loren. 1982. Computer rendering of stochastic models. *Communications of the ACM*, **25**(6), 371–384. Publisher: ACM New York, NY, USA.
- Furniss, Michael J. 2010. *Water, climate change, and forests: watershed stewardship for a changing climate*. DIANE Publishing.
- Gleason, Kelly E, Nolin, Anne W, & Roth, Travis R. 2013. Charred forests increase snowmelt: Effects of burned woody debris and incoming solar radiation on snow ablation. *Geophysical Research Letters*, **40**(17), 4654–4661. Publisher: Wiley Online Library.
- Gleeson, Tom, Smith, Leslie, Moosdorf, Nils, Hartmann, Jens, Dürr, Hans H, Manning, Andrew H, van Beek, Ludovicus PH, & Jelinek, A Mark. 2011. Mapping permeability over the surface of the Earth. *Geophysical Research Letters*, **38**(2). Publisher: Wiley Online Library.
- Hallema, Dennis W, Sun, Ge, Bladon, Kevin D, Norman, Steven P, Caldwell, Peter V, Liu, Yongqiang, & McNulty, Steven G. 2017. Regional patterns of postwildfire

- streamflow response in the Western United States: The importance of scale-specific connectivity. *Hydrological Processes*, **31**(14), 2582–2598. Publisher: Wiley Online Library.
- Hallema, Dennis W, Sun, Ge, Caldwell, Peter V, Norman, Steven P, Cohen, Erika C, Liu, Yongqiang, Bladon, Kevin D, & McNulty, Steven G. 2018. Burned forests impact water supplies. *Nature communications*, **9**(1), 1–8. Publisher: Nature Publishing Group.
- Harpold, Adrian A., Biederman, Joel A., Condon, Katherine, Merino, Manuel, Korgaonkar, Yoganand, Nan, Tongchao, Sloat, Lindsey L., Ross, Morgan, & Brooks, Paul D. 2014. Changes in snow accumulation and ablation following the Las Conchas Forest Fire, New Mexico, USA: CHANGES IN SNOW FOLLOWING FIRE. *Ecohydrology*, **7**(2), 440–452.
- IDEQ. 2002. South Fork Salmon River Subbasin Assessment. *Idaho Department of Environmental Quality*.
- Johansen, Mathew P, Hakonson, Thomas E, & Breshears, David D. 2001. Post-fire runoff and erosion from rainfall simulation: contrasting forests with shrublands and grasslands. *Hydrological processes*, **15**(15), 2953–2965. Publisher: Wiley Online Library.
- Jones, Jim E, & Woodward, Carol S. 2001. Newton–Krylov-multigrid solvers for large-scale, highly heterogeneous, variably saturated flow problems. *Advances in Water Resources*, **24**(7), 763–774. Publisher: Elsevier.
- Kinoshita, Alicia M, & Hogue, Terri S. 2011. Spatial and temporal controls on post-

- fire hydrologic recovery in Southern California watersheds. *Catena*, **87**(2), 240–252. Publisher: Elsevier.
- Kinoshita, Alicia M, & Hogue, Terri S. 2015. Increased dry season water yield in burned watersheds in Southern California. *Environmental Research Letters*, **10**(1), 014003.
- Kinoshita, Alicia M., Chin, Anne, Simon, Gregory L., Briles, Christy, Hogue, Terri S., O’Dowd, Alison P., Gerlak, Andrea K., & Albornoz, Alejandra Uribe. 2016. Wild-fire, water, and society: Toward integrative research in the “Anthropocene”. *Anthropocene*, **16**(Dec.), 16–27.
- Kollet, Stefan J, & Maxwell, Reed M. 2006. Integrated surface–groundwater flow modeling: A free-surface overland flow boundary condition in a parallel groundwater flow model. *Advances in Water Resources*, **29**(7), 945–958. Publisher: Elsevier.
- Kollet, Stefan J, & Maxwell, Reed M. 2008. Capturing the influence of groundwater dynamics on land surface processes using an integrated, distributed watershed model. *Water Resources Research*, **44**(2). Publisher: Wiley Online Library.
- Larsen, Isaac J, MacDonald, Lee H, Brown, Ethan, Rough, Daniella, Welsh, Matthew J, Pietraszek, Joseph H, Libohova, Zamir, de Dios Benavides-Solorio, Juan, & Schaffrath, Keelin. 2009. Causes of post-fire runoff and erosion: Water repellency, cover, or soil sealing? *Soil Science Society of America Journal*, **73**(4), 1393–1407. Publisher: Wiley Online Library.
- Lavee, H, Kutiel, P, Segev, M, & Benyamini, Y. 1995. Effect of surface roughness on

- runoff and erosion in a Mediterranean ecosystem: the role of fire. *Geomorphology*, **11**(3), 227–234. Publisher: Elsevier.
- Littell, Jeremy S., Peterson, David L., Riley, Karin L., Liu, Yongquiang, & Luce, Charles H. 2016. A review of the relationships between drought and forest fire in the United States. *Global Change Biology*, **22**(7), 2353–2369.
- Lundquist, Jessica D, Dickerson-Lange, Susan E, Lutz, James A, & Cristea, Nicoleta C. 2013. Lower forest density enhances snow retention in regions with warmer winters: A global framework developed from plot-scale observations and modeling. *Water Resources Research*, **49**(10), 6356–6370. Publisher: Wiley Online Library.
- López-Vicente, Manuel, & Martínez-Murillo, Juan F. 2016. Modelling hydrological connectivity in burned areas. A case study from South of Spain. Publisher: FuegoRED (Red Temática Nacional Efectos de los Incendios Forestales sobre el
- Ma, Qin, Bales, Roger C., Rungee, Joseph, Conklin, Martha H., Collins, Brandon M., & Goulden, Michael L. 2020. Wildfire controls on evapotranspiration in California's Sierra Nevada. *Journal of Hydrology*, **590**(Nov.), 125364.
- Maia, P., Pausas, J.G., Arcenogui, V., Guerrero, C., Pérez-Bejarano, A., Mataix-Solera, J., Varela, M.E.T., Fernandes, I., Pedrosa, E.T., & Keizer, J.J. 2012. Wildfire effects on the soil seed bank of a maritime pine stand — The importance of fire severity. *Geoderma*, **191**(Dec.), 80–88.
- Maina, Fadji Zaoua, & Siirila-Woodburn, Erica R. 2019. Watersheds dynamics following wildfires: Nonlinear feedbacks and implications on.

- Martin, Deborah A. 2016. At the nexus of fire, water and society. *Philosophical Transactions of the Royal Society B: Biological Sciences*, **371**(1696), 20150172.
- Maxwell, Jordan D., Call, Anson, & St. Clair, Samuel B. 2019. Wildfire and topography impacts on snow accumulation and retention in montane forests. *Forest Ecology and Management*, **432**(Jan.), 256–263.
- Maxwell, Reed M. 2013. A terrain-following grid transform and preconditioner for parallel, large-scale, integrated hydrologic modeling. *Advances in Water Resources*, **53**, 109–117. Publisher: Elsevier.
- Maxwell, Reed M, & Miller, Norman L. 2005. Development of a coupled land surface and groundwater model. *Journal of Hydrometeorology*, **6**(3), 233–247.
- Maxwell, RM, Condon, LE, & Kollet, SJ. 2015. A high-resolution simulation of groundwater and surface water over most of the continental US with the integrated hydrologic model ParFlow v3. *Geoscientific model development*, **8**(3), 923–937. Publisher: Copernicus GmbH.
- McGarigal, Kevin. 2015. FRAGSTATS help. *University of Massachusetts: Amherst, MA, USA*, 182.
- Mikkelsen, K. M., Maxwell, R. M., Ferguson, I., Stednick, J. D., McCray, J. E., & Sharp, J. O. 2013. Mountain pine beetle infestation impacts: modeling water and energy budgets at the hill-slope scale: PINE BEETLE IMPACTS ON THE WATER AND ENERGY BUDGET. *Ecohydrology*, **6**(1), 64–72.
- Moody, John A., & Martin, Deborah A. 2001. Initial hydrologic and geomorphic

- response following a wildfire in the Colorado Front Range. *Earth Surface Processes and Landforms*, **26**(10), 1049–1070.
- Moody, John A, Martin, Deborah A, Haire, Sandra L, & Kinner, David A. 2008. Linking runoff response to burn severity after a wildfire. *Hydrological Processes: An International Journal*, **22**(13), 2063–2074. Publisher: Wiley Online Library.
- Moody, John A, Shakesby, Richard A, Robichaud, Peter R, Cannon, Susan H, & Martin, Deborah A. 2013. Current research issues related to post-wildfire runoff and erosion processes. *Earth-Science Reviews*, **122**, 10–37. Publisher: Elsevier.
- Moody, John A, Ebel, Brian A, Nyman, Petter, Martin, Deborah A, Stoof, Cathelijne, & McKinley, Randy. 2015. Relations between soil hydraulic properties and burn severity. *International Journal of Wildland Fire*, **25**(3), 279–293. Publisher: CSIRO Publishing.
- Mote, Philip W., Li, Sihan, Lettenmaier, Dennis P., Xiao, Mu, & Engel, Ruth. 2018. Dramatic declines in snowpack in the western US. *npj Climate and Atmospheric Science*, **1**(1), 2.
- Murphy, Brendan P., Czuba, Jonathan A., & Belmont, Patrick. 2019. Post-wildfire sediment cascades: A modeling framework linking debris flow generation and network-scale sediment routing. *Earth Surface Processes and Landforms*, **44**(11), 2126–2140.
- Onda, Yuichi, Dietrich, William E., & Booker, Fred. 2008. Evolution of overland flow after a severe forest fire, Point Reyes, California. *CATENA*, **72**(1), 13–20.

- O'Neill, Mary MF, Tijerina, Danielle T, Condon, Laura E, & Maxwell, Reed M. 2020. Assessment of the ParFlow-CLM CONUS 1.0 integrated hydrologic model: Evaluation of hyper-resolution water balance components across the contiguous United States. *Geoscientific Model Development Discussions*, 1–50. Publisher: Copernicus GmbH.
- Ortíz-Rodríguez, Azalea Judith, Muñoz-Robles, Carlos, & Borselli, Lorenzo. 2019. Changes in connectivity and hydrological efficiency following wildland fires in Sierra Madre Oriental, Mexico. *Science of The Total Environment*, **655**(Mar.), 112–128.
- Palmer, Michael W. 1992. The coexistence of species in fractal landscapes. *The American Naturalist*, **139**(2), 375–397. Publisher: University of Chicago Press.
- Penn, Colin A., Bearup, Lindsay A., Maxwell, Reed M., & Clow, David W. 2016. Numerical experiments to explain multiscale hydrological responses to mountain pine beetle tree mortality in a headwater watershed. *Water Resources Research*, **52**(4), 3143–3161.
- Poon, Patrick K., & Kinoshita, Alicia M. 2018. Spatial and temporal evapotranspiration trends after wildfire in semi-arid landscapes. *Journal of Hydrology*, **559**(Apr.), 71–83.
- Radeloff, Volker C, Hammer, Roger B, Stewart, Susan I, Fried, Jeremy S, Holcomb, Sherry S, & McKeefry, Jason F. 2005. The wildland–urban interface in the United States. *Ecological applications*, **15**(3), 799–805. Publisher: Wiley Online Library.
- Reaney, SM, Bracken, Louise J, & Kirkby, MJ. 2014. The importance of surface controls on overland flow connectivity in semi-arid environments: Results from a

- numerical experimental approach. *Hydrological Processes*, **28**(4), 2116–2128. Publisher: Wiley Online Library.
- Sankey, Joel B., Kreitler, Jason, Hawbaker, Todd J., McVay, Jason L., Miller, Mary Ellen, Mueller, Erich R., Vaillant, Nicole M., Lowe, Scott E., & Sankey, Temuulen T. 2017. Climate, wildfire, and erosion ensemble foretells more sediment in western USA watersheds: Future Fire and Sediment. *Geophysical Research Letters*, **44**(17), 8884–8892.
- Santi, P. M., Hewitt, K., VanDine, D. F., & Barillas Cruz, E. 2011. Debris-flow impact, vulnerability, and response. *Natural Hazards*, **56**(1), 371–402.
- Saura, Santiago, & Martínez-Millán, Javier. 2000. Landscape patterns simulation with a modified random clusters method. *Landscape ecology*, **15**(7), 661–678. Publisher: Springer.
- Seibert, Jan, & van Meerveld, H.J. Ilja. 2016. Hydrological change modeling: Challenges and opportunities: Invited Commentary. *Hydrological Processes*, **30**(26), 4966–4971.
- Seibert, Jan, McDonnell, Jeffrey J., & Woodsmith, Richard D. 2010. Effects of wildfire on catchment runoff response: a modelling approach to detect changes in snow-dominated forested catchments. *Hydrology Research*, **41**(5), 378–390.
- Shakesby, R., & Doerr, S. 2006. Wildfire as a hydrological and geomorphological agent. *Earth-Science Reviews*, **74**(3-4), 269–307.
- Shakesby, RA, Doerr, SH, & Walsh, RPD. 2000. The erosional impact of soil hy-

- drophobicity: current problems and future research directions. *Journal of hydrology*, **231**, 178–191. Publisher: Elsevier.
- Spigel, Kevin M., & Robichaud, Peter R. 2007. First-year post-fire erosion rates in Bitterroot National Forest, Montana. *Hydrological Processes*, **21**(8), 998–1005.
- Uecker, Ted M, Kaspari, Susan D, Musselman, Keith N, & McKenzie Skiles, S. 2020. The Post-Wildfire Impact of Burn Severity and Age on Black Carbon Snow Deposition and Implications for Snow Water Resources, Cascade Range, Washington. *Journal of Hydrometeorology*, **21**(8), 1777–1792.
- USDA. 2000. South Fork Salmon Subbasin Review. *Boise National Forest and Payette National Forest*.
- Wester, Thad, Wasklewicz, Thad, & Staley, Dennis. 2014. Functional and structural connectivity within a recently burned drainage basin. *Geomorphology*, **206**(Feb.), 362–373.
- Westerling, A. L. 2006. Warming and Earlier Spring Increase Western U.S. Forest Wildfire Activity. *Science*, **313**(5789), 940–943.
- Westerling, Anthony LeRoy. 2016. Increasing western US forest wildfire activity: sensitivity to changes in the timing of spring. *Philosophical Transactions of the Royal Society B: Biological Sciences*, **371**(1696), 20150178.
- Williams, C. Jason, Pierson, Frederick B., Robichaud, Peter R., Al-Hamdan, Osama Z., Boll, Jan, & Strand, Eva K. 2016. Structural and functional connectivity as a driver of hillslope erosion following disturbance. *International Journal of Wildland Fire*, **25**(3), 306.

- Wilson, Codie, Kampf, Stephanie K., Ryan, Sandra, Covino, Tim, MacDonald, Lee H., & Gleason, Hunter. 2021. Connectivity of post-fire runoff and sediment from nested hillslopes and watersheds. *Hydrological Processes*, **35**(1).
- Wine, Michael L., Makhnin, Oleg, & Cadol, Daniel. 2018. Nonlinear Long-Term Large Watershed Hydrologic Response to Wildfire and Climatic Dynamics Locally Increases Water Yields. *Earth's Future*, **6**(7), 997–1006.

APPENDIX A:
METEOROLOGICAL FORCINGS

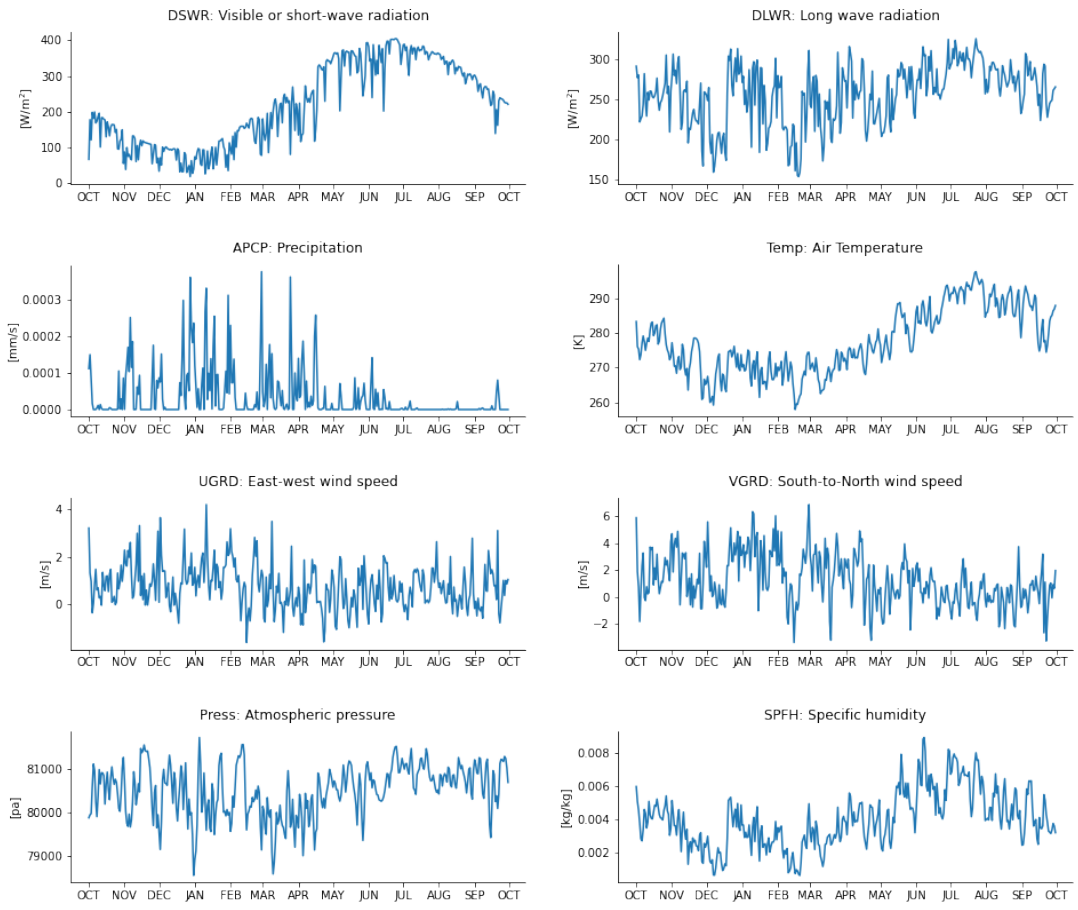


Figure A.1: Time series' of mean daily values for each of the eight meteorological forcings used by ParFlow-CLM.

APPENDIX B:
POSTFIRE LANDSCAPES

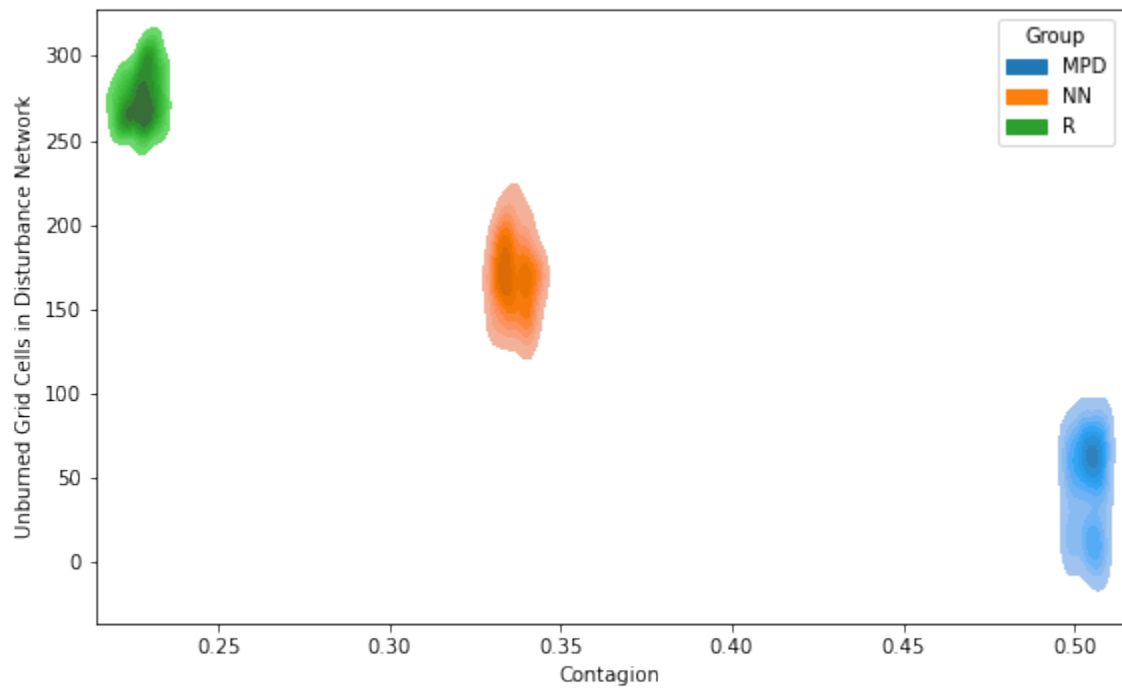


Figure B.1: Bivariate kernel density estimation plot relating the distribution of contagion values for each experimental group (R, NN, MPD) to the distribution of unburned grid cells contained in their disturbance flow path networks.



Figure B.2: Map of the disturbance flow path network for each fire mosaic in Group R in ascending order according to the number of unburned grid cells in the network. The brackets above each map show the number of unburned grid cells (left) and the contagion value (right).



Figure B.3: Map of the disturbance flow path network for each fire mosaic in Group NN in ascending order according to the number of unburned grid cells in the network. The brackets above each map show the number of unburned grid cells (left) and the contagion value (right).



Figure B.4: Map of the disturbance flow path network for each fire mosaic in Group MPD in ascending order according to the number of unburned grid cells in the network. The brackets above each map show the number of unburned grid cells (left) and the contagion value (right).

APPENDIX C:
GITHUB REPOSITORY

Preprocessing, modeling, and postprocessing scripts used in this project are available in a public GitHub repository at:

`https://github.com/luketelfer/ms-appendix-c`

We have also included a few datasets containing select model outputs. Table C.1 provides a road map to the repository with brief descriptions of the files and directories contained within.

Table C.1: GitHub repository road map.

| | |
|--|--|
| [1] Preprocessing: Scripts and Data | |
| <code>flow_tracing.py</code> | Python functions for delineating flow paths and other watershed characteristics. |
| <code>generate_mosaics.py</code> | Python functions for generating NLM landscapes. |
| <code>mosaic_to_pfclm.py</code> | Python functions for converting NLM landscapes to ParFlow indicator and CLM input files. |
| <code>template_indicator.pfb</code> | ParFlow indicator file template. |
| <code>template_vegm.dat</code> | CLM input file template. |

| | |
|--|--|
| [2] ParFlow-CLM: Scripts and Data | |
| <code>domain_inputs/</code> | Directory containing ParFlow-CLM domain input files used in all simulations. |
| <code>exp_inputs/</code> | Directory containing simulation-specific ParFlow-CLM input files. |
| <code>tcl_scripts/</code> | Directory containing TCL scripts used to set up and execute ParFlow-CLM model runs. |
| <code>wrf_forcings.tar.gz</code> | Directory containing spatially uniform meteorological forcings (WY2006) used in all simulations. |

| | |
|------------------------------------|---|
| [3] Postprocessing: Scripts | |
| <code>pfpostproc/</code> | Python module directory containing postprocessing calculations, attributes, functions, and workflows. |
| <code>run_ctr_postproc.py</code> | Python script used to execute postprocessing workflow for baseline control simulations. |
| <code>run_exp_postproc.py</code> | Python script used to execute postprocessing workflow for experiment simulations. |

| | |
|---|--|
| [4] Results: Model Outputs and Domain Data | |
| <code>ctr_results.nc</code> | NetCDF file containing model outputs (ET, runoff, soil water storage, SWE) for baseline control simulations. |
| <code>domain_data.nc</code> | NetCDF file containing maps of domain characteristics. |
| <code>exp_mosaics.tar.gz</code> | NetCDF file containing mosaic maps and spatial metrics for all experiments. |
| <code>exp_results/</code> | Zarr store containing model outputs (ET, runoff, soil water storage, SWE) for experiment simulations. |
